atmosphere

MDPI

Article

Polar Winds: Airborne Doppler Wind Lidar Missions in the Arctic for Atmospheric Observations and Numerical Model Comparisons

Steven Greco [1,*], George D. Emmitt [1], Alice DuVivier [2], Keith Hines [3] and Michael Kavaya [4]

1 Simpson Weather Associates, Charlottesville, VA 22902, USA; gde@swa.com
2 National Center for Atmospheric Research, Boulder, CO 80307, USA; duvivier@ucar.edu
3 Byrd Polar and Climate Research Center, The Ohio State University, Columbus, OH 43210, USA; hines.91@osu.edu
4 NASA Langley Research Center, Hampton, VA 23681, USA; michael.j.kavaya@nasa.gov
* Correspondence: sxg@swa.com; Tel.: +1-434-979-3571

Received: 21 September 2020; Accepted: 14 October 2020; Published: 22 October 2020

Abstract: During October–November 2014 and May 2015, NASA sponsored and conducted a pair of airborne campaigns called Polar Winds to investigate atmospheric circulations, particularly in the boundary layer, over the Arctic using NASA's Doppler Aerosol WiNd (DAWN) lidar. A description of the campaigns, the DAWN instrument, wind retrieval methods and data processing is provided. During the campaigns, the DAWN instrument faced backscatter sensitivity issues in the low aerosol conditions that were fairly frequent in the 2–6 km altitude range. However, when DAWN was able to make measurements, comparisons with dropsondes show good agreement and very low bias and supports the use of an airborne Doppler wind lidar such as DAWN that can provide profiles with high velocity precision, ~65 m vertical resolution and horizontal spacing as fine as 3–7 km. Case study analyses of a Greenland tip jet, barrier winds and an upper level jet are presented and show how, despite sensitivity issues, DAWN data can be confidently used in diagnostic studies of dynamic features in the Arctic. Comparisons with both an operational and research Weather Research and Forecasting (WRF) model for these events also show the potential for utilization in model validation. The sensitivity issues of the DAWN laser have since been corrected.

Keywords: airborne Doppler wind lidar; Polar Winds field campaigns; DAWN; wind retrieval; wind profiles; boundary layer; arctic; tip jet; barrier winds; WRF

1. Introduction

Over the past twenty years, rising air and sea surface temperatures and shrinking sea ice extent in the Arctic [1] have led to a growing scientific interest in the atmospheric processes of the globe's polar regions and the ability to better observe, model and forecast these processes on time scales from hours to seasonal. Unfortunately, the existing conventional observation network needed to accomplish this in the polar regions, particularly in the Arctic and over the ice and the open waters, remains sparse and limited.

With this as a motivation, there have been numerous ship-based [2] and airborne [3–10] field campaigns to address this observational data gap as well as study the atmospheric processes over the Arctic. Most recently, the WMO World Weather Research Program (WWRP) Polar Prediction Program coordinated and has been shepherding an international multi-year activity called the Year of Polar Prediction (YOPP) [11] with intensive observations, modeling and verification in the Arctic and Antarctic during 2017–2019. In addition, the year-long international research expedition

Multidisciplinary Drifting Observatory for the Study of Arctic Climate (MOSAiC) was launched in the fall of 2019 and includes ship-based, land-based and airborne measurements of the Arctic [12].

One instrument that has been used and proved beneficial to previous airborne campaigns and the study of the Arctic atmosphere is the Airborne Doppler Wind Lidar (ADWL) [3,5,6,9,13]. Prior to the intensive YOPP, NASA sponsored and conducted a pair of airborne campaigns to, in part, investigate atmospheric circulations in the Arctic, specifically the Planetary Boundary Layer (PBL), over and off the coast of Greenland using an ADWL. These campaigns, collectively called Polar Winds, were designed to fly the Doppler Aerosol WiNd (DAWN) lidar [14] to take airborne wind and aerosol measurements of the Arctic atmosphere and PBL during October–November 2014 and May 2015.

This paper will focus on the DAWN wind measurements taken during the campaigns, particularly the characterization of the atmospheric flow and the verification/validation the observations provide for numerical models. In the following sections, we will provide an overview of the scientific campaigns and their objectives, a description of the instruments, DAWN data processing and utility, comparisons with co-located dropsondes and a presentation of case study analysis and model validation results.

2. Field Campaigns

The Polar Winds airborne field campaigns were designed in part to utilize DAWN and dropsondes to investigate the atmospheric circulations over and off the coasts of Greenland and over the Denmark Strait between Greenland and Iceland. This included a series of missions designed to measure the winds and aerosols associated with barrier winds, tip jets and other boundary layer features. In addition to collecting data to study these circulations, one of the most important objectives of the two campaigns was to generate a data set of high-resolution 3-dimensional winds from DAWN that could be used for the validation of polar atmospheric numerical models.

Another component of Polar Winds were calibration and validation (cal/val) missions or flight segments to underfly both existing remote sensing instruments (i.e., Cloud-Aerosol Lidar and Infrared Pathfinder (CALIPSO), MODerate-resolution Imaging Spectroradiometer (MODIS) or Advanced Scatterometer (ASCAT)) and, at the time of the campaign, to practice underflying the future Aeolus Airborne Demonstrator for the Direct-Detection Doppler Wind Lidar (ALADIN) that was launched on 22 August 2018. To achieve this objective, NASA flew seven missions in May 2015 in coordination with the German Aerospace Research Establishment Deutsches Zentrum für Luft- und Raumfahrt (DLR) Falcon aircraft that was equipped with both a coherent detection airborne wind lidar and a direct detection wind lidar that is an Aeolus simulator. During these missions, both DAWN and the Falcon ADWLs were flown to simulate the orbits and scanning of Aeolus and to take measurements that would benefit future development, planning and validation. This "space-based" component of Polar Winds will be the subject of a separate publication but has also been documented by Marksteiner et al., 2018.

Polar Winds campaign 1 (hereafter called PW1) was based in Kangerlussuaq, Greenland and flew DAWN on board the NASA King Air Utility Cargo 12B (UC-12B) during October–November 2014. Table 1 lists a summary of the PW1 missions with the mission flight tracks show in Figure 1. Polar Winds campaign 2 (hereafter called PW2) was based in Keflavik, Iceland and utilized the NASA Douglas Craft-8(DC-8) to fly DAWN and the Yankee Environmental Services (YES) High Definition Sounding System (HDSS)/eXpendable Digital Dropsondes (XDD) [15] over the Arctic in May 2015. The mission descriptions and flight tracks for PW2 are shown, respectively, in Table 2 and Figure 1. In total, twenty-four individual missions with over 80 h of research flights were flown during PW1 and PW2.

Table 1. Mission flights and science objectives during PW1.

Mission Number	Date	Time (GMT)	Science Objectives
1	10/29/14	1151–1347	Ice–land–water boundary layer
2	10/29/14	1456–1643	CALIPSO underflight; Marine boundary layer
3	10/30/14	1323–1642	Land–water; west coast of Greenland; Aeolus simulation
4	10/31/14	1101–1919	Tip jet; Land–ice cap transect; Aeolus simulation
5	11/3/14	1356–1714	Offshore transects; CALIPSO/ASCAT underflight
6	11/4/14	1358–1727	Land–water boundary layer; Aeolus simulation; MODIS underflight
7	11/5/14	1411–1721	Land–ice cap edge; Cloud layers
8	11/6/14	1405–1631	Marine boundary layer; Aeolus simulation; MODIS underflight
9	11/7/14	1411–1648	Boundary layer (land–water)
10	11/8/14	1554–1913	Coastal katabatic flow; MODIS/ASCAT underflight
11	11/10/14	1428–1700	Coastal boundary layer (rolls); CALIPSO/ASCAT underflight
12	11/11/14	1407–1717	Land–marine boundary layer
13	11/12/14	1106–1854	Tip jet/winds; off-shore transect
14	11/13/14	1403–1625	All land/ice cap boundary layer

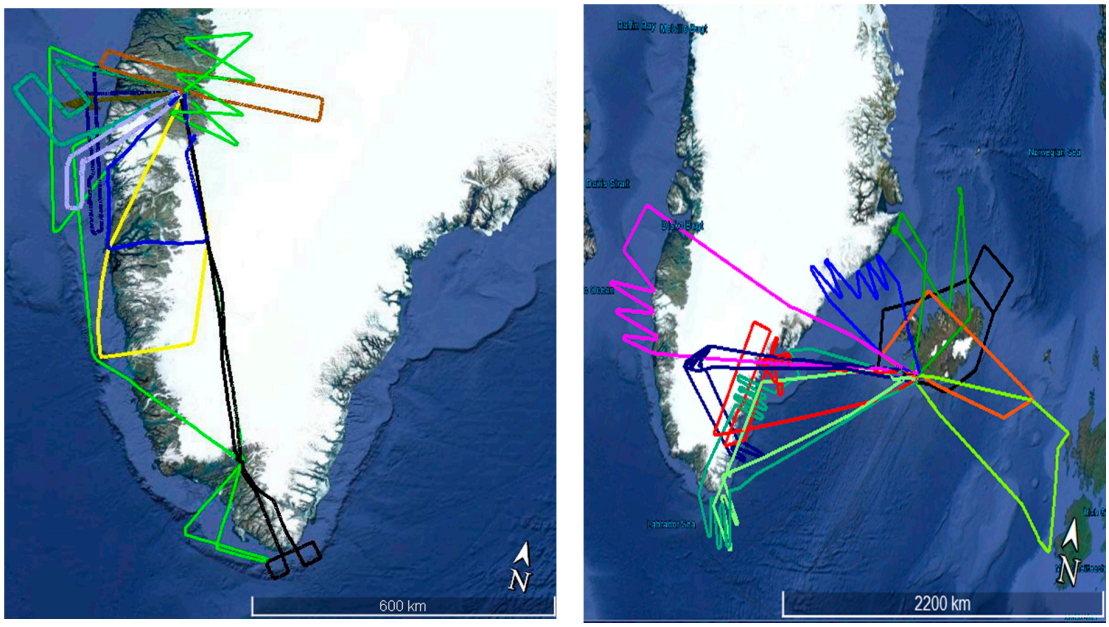

Figure 1. Mission flight paths for PW1 (**left**) and PW2 (**right**) (Google Earth).

Table 2. Mission flights and science objectives during PW2.

Mission Number	Date	Time (GMT)	Science Objectives
1	5/11/15	1318–1720	Around Iceland
2	5/13/15 *	1057–1503	TechDemoSat 1 underpass
3	5/15/15 *	1604–2006	North Atlantic upper jet stream
4	5/16/15 *	1357–2106	Aeolus cal/val flight; southern Greenland
5	5/17/15	1352–2109	Tip jet and katabatic flow off east coast of Greenland
6	5/19/15 *	1200–1702	Tip jet, Coastal upper jet; Aeolus cal/val flight
7	5/21/15	1742–2151	Barrier winds
8	5/23/15 *	1354–1955	Southeast coast of Greenland; ice, land and water transects Aeolus cal/val flight
9	5/24/15	1153–1822	Coastal zone off west coast of Greenland
10	5/25/15 *	1407–1716	Around Iceland; Upper jet; Aeolus cal/val flight

* Coordinated with DLR Falcon.

Numerical Models

Given the sparse conventional observation network in the Polar regions, perhaps the best source of routine wind data over the Arctic water and ice comes from reanalyses and model forecast data. Several advanced global reanalyses are available, such as the European Centre for Medium-Range Weather Forecasts (ECMWF) Reanalysis-Interim (ERA-I), the Climate Forecast System Reanalysis, and ERA-5 [16,17]. The regional Arctic System Reanalysis (ASR), however, has the high resolution to capture mesoscale wind structures along the coast of Greenland that are missed with lower resolution [18]. The ASR [19] and the ASR Version 2 [18] provide atmospheric variables on the mesoscale resolution of 15 km and 3 h. In addition to the reanalyses, the Weather Research and Forecast Model (WRF) model [20] and the WRF model optimized for polar conditions by the Byrd Polar and Climate Research Center at The Ohio State University (OSU) and referred to as the Polar WRF [21,22] have also been used to investigate the low-level circulations of the Arctic over various land surface types (ice sheet, water, land, transition zones). WRF and Polar WRF can be used for operational forecasts, climate applications, and case studies (e.g., [18,23,24]).

The model used operationally for Polar Winds was WRF version 3.6.1 with the Polar WRF optimizations for high latitude applications. In addition to operational Polar WRF forecasts run during the Polar Winds campaigns, we used the WRF Model, version 3.7.1 for a case study of the barrier wind event of 21 May 2015 using features and parameterization schemes specifically based on sensitivity study analyses for barrier wind conditions [24]. These latter model forecasts are used in our barrier wind case study presented in Section 4. The horizontal domains of the two models are shown in Figure 2 while a comparison of the features of the two models is shown in Table 3.

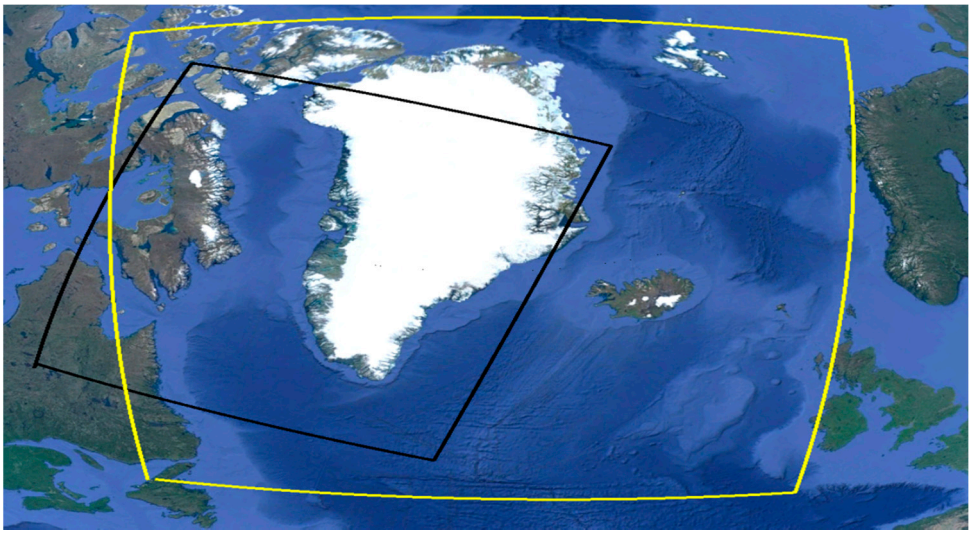

Figure 2. Horizontal domains of the Polar WRF run operationally during PW1 (black) and the research WRF model that was run post PW2 to study barrier winds (yellow).

Table 3. WRF Specifications and Parameterizations used in this study.

WRF Scheme/Feature	OSU Polar WRF PW1/PW2	WRF Version 3.7.1 PW2
Initialization Time	Twice daily (00Z/12Z)	00Z
Boundary Conditions	NCEP GFS (28 km)	ECMWF ERA-I (70 km)
Horizontal Resolution	8 km	5 km
Vertical Levels	49	60
Sea Ice Thickness	1.5 m	0.5 m
Longwave Radiation	RRTMG	RRTMG
Shortwave Radiation	RRTMG	RRTMG
Cumulus Param.	Grell-3	Kain–Fritsch
Microphysics	Morrison	Morrison
Surface Layer	MYJ	Revised MM5
Land Surface Model	Noah	Noah
Planetary Boundary Layer Scheme	MYJ	UW

3. The DAWN Instrument and Wind Profile Retrieval Methods

3.1. Instrument Description and Specifications

The featured instrument for the wind measurements taken during Polar Winds was the DAWN airborne wind lidar, which was both designed and built at NASA Langley Research Center (LaRC) [14,25,26]. Prior to Polar Winds, DAWN had been deployed on a NASA DC-8 aircraft during the 2010 Genesis and Rapid Intensification Processes (GRIP) [14] and as a ground-based instrument in field demonstrations to measure off-shore winds off the coast of Virginia [27,28]. Since Polar Winds, DAWN has also been flow on the NASA DC-8 during the 2017 Convective Processes Experiment (CPEX) [29] and the recent 2019 Aeolus Ca/Val Test Flight campaign based out of Palmdale, CA and Hawaii [30].

Table 4 provides a brief summary of the DAWN specifications, system parameters and measurement statistics at the time of the campaigns, which have been presented in more detail in previous DAWN publications [14,29]. At a wavelength of 2.05 microns and at 250 mJ per pulse, DAWN was designed to be the most "capable' ADWL available for airborne science missions. "Capable" is defined by high horizontal and vertical resolution, ~100X better aerosol backscatter sensitivity than prior ADWLs, >100 m/s wind velocity capture (search) bandwidth, and minimum probability of outlier wind estimates.

Table 4. DAWN Wind Lidar Specifications during Polar Winds.

Attribute	Value
Airplanes flown	DC-8 and UC-12B
Solid-state laser crystal and wavelength	Holmium Thulium Lutetium Lithium Fluoride (Ho:Tm:LuLiF), 2.053472 microns
Laser pulse energy, rate, and Full Width Half Max (FWHM) duration	250 mJ, 10 Hz, 180 ns (PW1); 100 mJ, 5 Hz, 180 ns (PW2)
Number of LOS/azimuth angles	Selectable; Only 2 and 5 angles used
Number of laser shots at each LOS	Selectable, typically 10–20 (1–2 s)
Optical detection	Dual-balanced coherent (heterodyne), Indium Gallium Arsenide (InGaAs)
Laser pointing knowledge	Dedicated Inertial Navigation System (INS)/Global Positioning System (GPS) on lidar supplemented with ground returns
Horizontal Resolution of Vertical Profile	3–10 km
Vertical Resolution of Vertical Profile	66 m

While the laser and receiver portions of the system are fixed, the manner in which the laser beam is scanned can be altered to meet mission requirements. The number of scanning angles can be chosen but only downward viewing is accommodated with only 2 and 5 scanning angles used during Polar Winds. The number of laser shots averaged at each angle is also selectable, trading horizontal resolution with minimum attenuated aerosol backscatter sensitivity.

3.2. DAWN Wind Profile Retrieval

The Line-Of-Sight (LOS) velocities computed from the DAWN signal return at multiple scanner azimuths are used to compute 3-dimesional (u, v, w) vertical profiles of winds. During Polar Winds, a vertical profile was derived in most instances from either a 2-point (90 degrees between stares) or 5-point (22.5 degrees between stares) scan with a 30.1 degree off nadir half angle. The dwells at each stare point varied from 1 to 4 s and the time to complete full step-stare conical scan for wind profiles is about 20–30 s. From these 90 degree sector conical scans, the basic wind profile was constructed with 66 m resolution in the vertical. The vertical resolution results from the nadir angle (fixed) and the duration (selectable) of the backscattered signal that is used to estimate each the LOS wind velocity. Given that the 2 μm backscatter in the polar regions was low and DAWN was operating at a reduced sensitivity, a LOS processing gate was set at ~153 m. For better resolution of backscatter gradients, each 153 m processing gate was advanced (slid) by 76.5 m, which provided the 66 m (66 m = cos(30) * 76.5 m) vertical resolution of the wind profiles.

The processing of ADWL data provides many challenges because of the effects of aircraft motion, scanning geometry, and the effects of the surface. To address these issues, processing algorithms have been developed for the DAWN system for the following:

1. Pointing Knowledge and Aircraft Motion Accounting—DAWN has its own GPS/INS and much effort is made to keep pointing errors below 1 degree. Navigation data from the DC-8 systems are combined with the DAWN navigation data to achieve the best results, especially with regard to well-known heading drifts.
2. Utilizing Surface Returns During Calibration Legs—We use ground returns in cloud-free conditions (below aircraft) during constant altitude flight segments over uniform terrain to calibrate the GPS/INS. The attitude corrections for pitch and yaw were determined by comparing the LOS velocity at the ground for each look angle of a scan with the value of 0 m/s, which should be the speed of the ground, and iteratively finding the optimum pitch and yaw correction that minimizes the mean difference between the LOS velocities at the ground and zero. Although the correction factors derived from the ground returns should be constant once determined, we find they can vary from one day to another. The results are a significant reduction in uncertainty in the LOS wind range profiles and the vertical profiles of all three components of the winds (u, v, and w).
3. Range Precision (Height Correction)—Adjusting the height assignment of range gated LOS data. The height adjustment, usually less than a few 10's of meters, is made empirically by "correcting" the reported time of flight from the lidar system. Strong aerosol gradients just adjacent to the surface may also cause a few meters of uncertainty to the range to ground values.

After accounting for these issues, the LOS values at each range gate are then used to process the 3-dimensional profiles. While the shortest possible range gate for DAWN is ~30 m, we have found that 76 m is optimum for processing. A sliding range gate of 38 m is also used to report the wind estimates along a LOS. Thus, there is some overlap between adjacent projected levels of ~32 m. The wind profiles are then determined by using a Levenberg–Marquardt (LM) algorithm to solve for u and v within each scan and are representative of averages taken over 2 or 5 stares and over the time it takes to complete the full scan (20–30 s). The resulting profile measurements determined in this fashion provided a wind vector every ~66 m in the vertical. Two quality tests set for the profiles are the minimum SNR for

individual LOS products and the Goodness of Fit (GOF) for the vector products derived from a best fit LM solver.

Table 5 provides a listing of these data measurements along with the precision and both horizontal and vertical resolution of the vertical profiles. The development of the data processing algorithms has resulted in high accuracy (<0.05 m/s) in the horizontal wind component observations and high resolution of aerosol features (<5 m in some instances). The maximum range of the DAWN varies depending on the amount of clouds and aerosols but can produce wind profiles (though not complete) from 8–12 km down to the surface. Three examples of the vertical profiles of LOS Signal to Noise Ratio (SNR), profile wind speed and direction during PW2 are provided in Figure 3. The top panel is for a profile over the North Atlantic Ocean and shows good measurement coverage in the upper part of the profile due to clouds and aerosols but the lack of aerosols and weak return signal (SNR) between 1 and 5 km prevented accurate measurements in that layer. However, there were enough aerosols below 1 km to allow accurate wind measurements in the boundary layer. The profiles presented in the middle and bottom of Figure 3 were taken over the Greenland ice sheet (terrain elevation of 2–2.5 km). When the return signal (SNR) was strong enough due to the presence of thin and broken cloud and/or aerosols, accurate measurements were obtained (bottom panel) but the low aerosol conditions frequently found above 1–2 km and below 5–6 km over the ice sheet often resulted in a return signal that was too weak (and poor GOF) for the computation of wind profiles.

Table 5. DAWN measurements, precision and resolutions.

LOS wind measurement precision	<1 m/s
u, v, w measurement precision	<1 m/s
Data product vertical resolution	75–150 m typical, selectable
Horizontal resolution of each LOS wind profile	500 m typical (variable with # shots)
Horizontal resolution of vertical profile of horizontal wind	3–12 km typ. (variable with # LOS, #shots, aircraft ground speed)

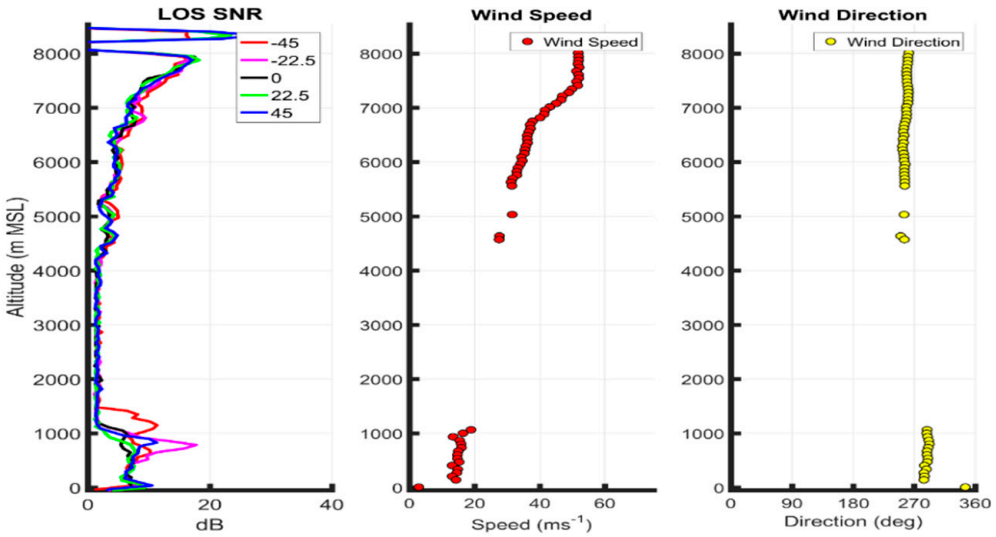

Figure 3. *Cont.*

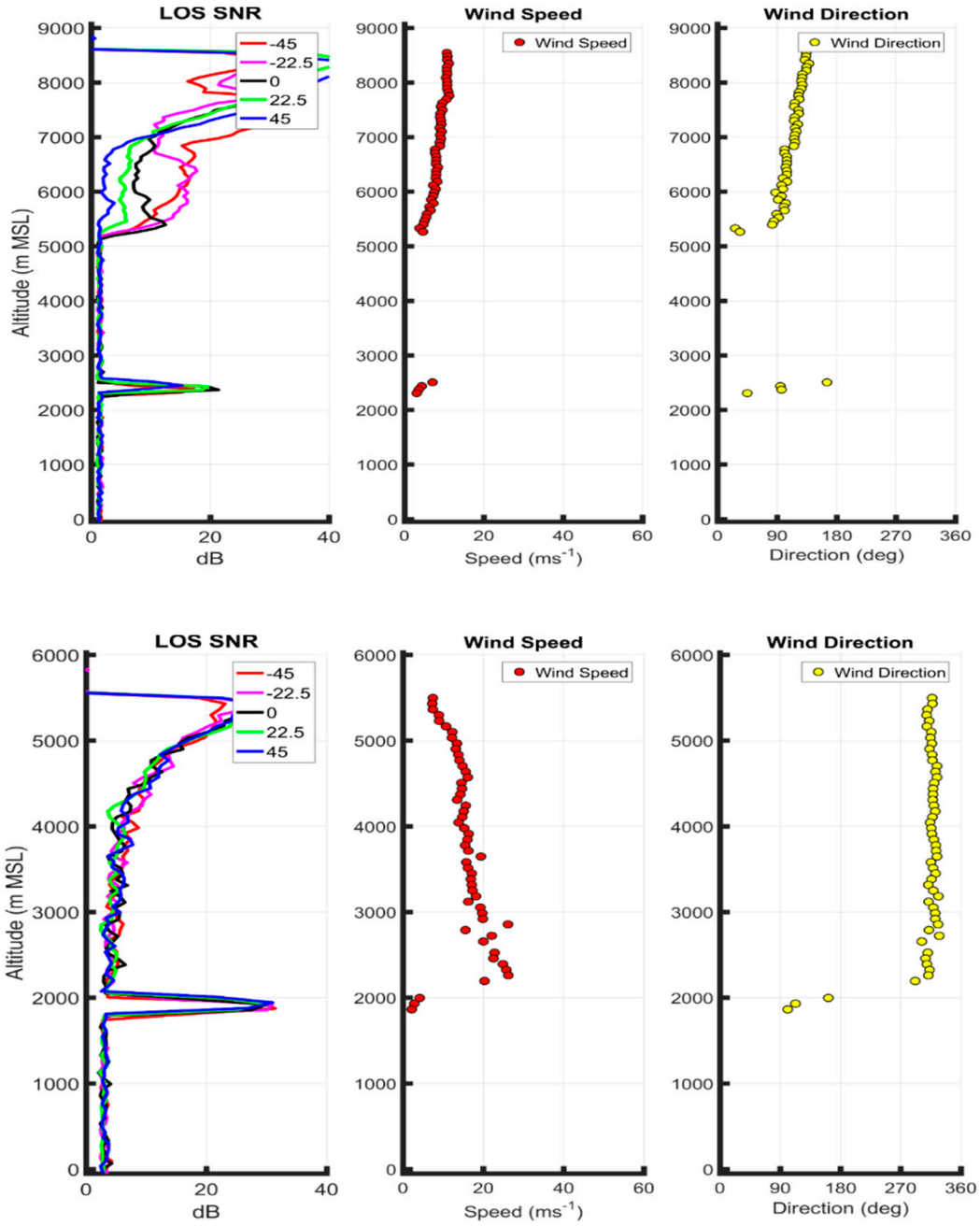

Figure 3. Examples of a Polar Winds profiles of LOS SNR, wind speed and wind direction from over the North Atlantic on 15 May 2015 18:05:35Z (**top**), and over the Greenland ice sheet on 16 May 2015 1511:37Z (**middle**) and 17 May 2015 15:36:37Z (**bottom**).

4. Results

Upon returning from the field campaigns, analysis of the DAWN raw data indicated that, during Polar Winds, DAWN performed less than ideally due to optical misalignment and reduced throughput efficiencies that have been corrected post-experiment. These issues lead to problems in obtaining full profiles, particularly in low aerosol situations common to near and over Greenland (PW1 and PW2) and over parts of the Arctic Ocean, Denmark Strait and north Atlantic (PW2), especially in the middle levels of 3–6 km above the surface. The top two panels of Figure 3, one taken over the North Atlantic and another taken over the Greenland ice sheet, are ideal examples of this. However, as seen in Figure 3, it will also be shown in the following sections that, aerosols permitting, fuller DAWN

profiles could be obtained and demonstrated close agreement with dropsondes and provided quality PBL and upper level data for numerical model (e.g., Polar WRF) validation and for the scientific study of atmospheric circulation such as low-level jets and barrier winds.

4.1. DAWN–Dropsonde Comparisons

Over the past twenty years, dropsondes have played a key role in airborne atmospheric profiling and have become the "truth" with which many satellite and airborne remote sensing instruments such as DAWN have been compared. As mentioned in Section 2, the YES HDSS/XDD dropsondes were launched from the DC-8 during all PW2 missions. Prior to Polar Winds, this system was used on the Navy's Twin Otter, the NASA Wallops Flight Facility P-3, and NASA's DC-8 and WB-57 aircraft [15]. Since the field campaigns, they have also been used during the 2015 Tropical Cyclone Intensity (TCI) experiment [31,32], and the 2017 CPEX [29,33].

During PW2, a total of 90 XDD dropsondes were attempted over the ten missions. A total of 66 DAWN–Dropsonde pairs were identified that had both a successful DAWN wind profile (over 1 km worth of data) and the dropsondes (occasionally, no wind were reported). Qualitative comparisons were made between the dropsondes and the closest (in time and space) DAWN wind profile along the flight track. Some of these comparisons will be shown in Section 4.2. In addition, for each successful DAWN measurement within a vertical profile, quantitative comparisons were made with the closest (in height) dropsonde observation. The results of these statistical comparisons for the entirety of PW2 are shown in the scatterplots for wind speed (WS) and wind direction (WD) comparisons in Figure 4, and statistics for the quantitative comparison of wind speed and direction for all of PW2, and subsetted by both height and wind speed in Table 6. In these tables, the comparisons are done for DAWN—dropsondes where mean Δz is the mean absolute height difference between the DAWN and dropsondes observation being compared, the bias is the mean difference of the DAWN and dropsonde wind speeds (ΔWS) and wind directions (ΔWD), and the Root Mean Square Difference (RMSD) is basically the standard deviation of the differences.

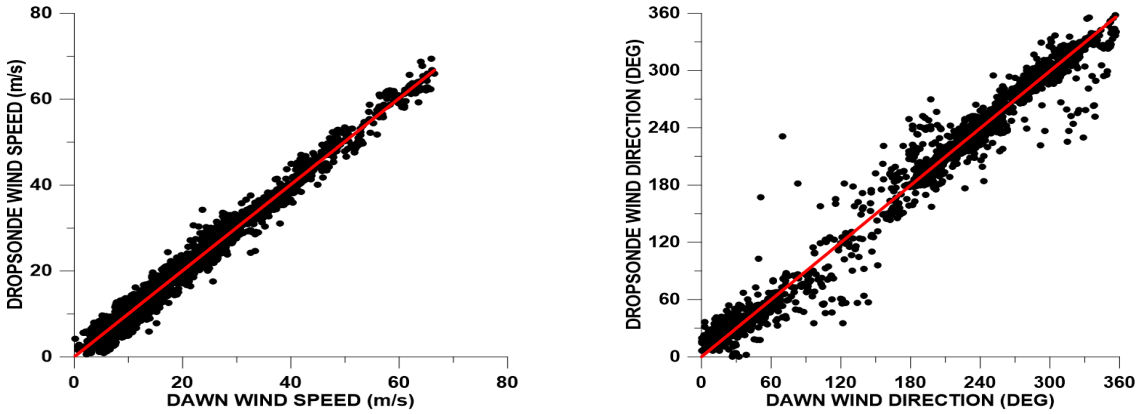

Figure 4. Scatterplots of DAWN–dropsonde comparisons of wind speed (**left**) and wind direction (**right**) for PW2.

Table 6. Quantitative comparisons of DAWN and dropsonde wind speed and wind direction during PW2 as subsetted by height (top) and DAWN wind speed (bottom).

Height Layer	Number of Comparisons	Δz (m)	Mean ΔWS (Bias)	RMSD ΔWS	Mean ΔWD (Bias)	RMSD ΔWD
ALL	2548	2.28	−0.01	1.98	−0.48	15.9
0–2.5 km	430	1.94	0.09	1.99	−0.48	18.0
2.5–5 km	812	2.00	0.48	1.23	−1.75	22.7
5.0–7.5 km	710	2.48	−0.14	1.85	−0.51	9.27
Above 7.5 km	596	2.64	−0.58	2.04	0.91	6.50
Wind Speed Range	**Number of Comparisons**	**Δz (m)**	**Mean ΔWS (Bias)**	**RMSD ΔWS**	**Mean ΔWD (Bias)**	**RMSD ΔWD**
ALL	2548	2.28	−0.01	1.98	−0.48	15.9
0–10 m/s	826	1.98	0.05	1.74	1.11	22.5
10–20 m/s	777	2.21	0.23	1.97	−2.40	10.3
20–30 m/s	452	2.64	−0.45	2.25	−0.23	6.25
Over 30 m/s	493	2.53	−0.08	2.06	0.32	1.68

It can be seen from Table 6 and Figure 4 that, when compared to the standard of the dropsondes, there were no major departures or bias between the two wind measuring systems. One potential reason for the higher difference/bias above 7.5 km is a height assignment delay in the dropsondes wind data reporting that may have impacted the comparisons in the upper level flights that sampled strong shear below the upper jet or wind maximums on several occasions. In general, both the wind lidar and dropsonde are subject to the time and space variability of the wind field during a sounding. The dropsonde, although traversing a volume of the atmosphere on a trajectory governed largely by the wind field, travels on a trajectory that is significantly different from the near instantaneous path of the laser beam. The two pathways are not coincident in time or space. Differences between the velocity measurements of the two systems may thus be real (excellent measurements) but represent different sampled volumes. Both observations are useful and can be considered representative of the flow. By analogy, these differences are similar to those between rain gauge measured and radar estimated precipitation totals.

4.2. Case Study Analyses

To illustrate the coverage, usefulness and viability of the DAWN data for scientific research and model validation in the Arctic, we briefly present and describe the results of three individual missions flown during Polar Winds. The first mission was the investigation of low-level barrier winds off the east coast of Greenland on 21 May 2015 during PW2 while the second mission presented is the sortie into a low-level jet off the southern tip of Greenland on 21 October 2014 during PW1. Analysis from the NASA DC-8 mission over an upper level cyclone and jet along the east coast of Greenland on 19 May 2015 during PW2 are also presented.

4.2.1. Barrier Wind Event during PW2 on 21 May 2015

The region off the southern and central eastern coast of Greenland and over the Denmark Strait is an area noted for strong low-level barrier winds as strong low-pressure systems move eastward towards and past Iceland and the northerly/northeasterly flow is blocked and channeled by the Greenland land mass resulting in strong low-level winds [34–37]. These winds have been investigated as part of the Greenland Flow Distortion Experiment (GFDex) [4] and the Norwegian International Polar Year-The Observing System. Research and Predictability Experiment (IPY-THORPEX) with an ADWL [5]. 21 May 2015 provided a prime example of this scenario as forecasted by the models and is shown in Figure 5. A PW2 mission was flown to gather high-resolution DAWN and Dropsonde wind data for

this case and to compare against each other and the models. The satellite image (from the Meteosat Second Generation Spinning Enhanced Visible and Infrared Imager (MSG-SEVIRI)), flight track and dropsonde locations are shown in Figure 6.

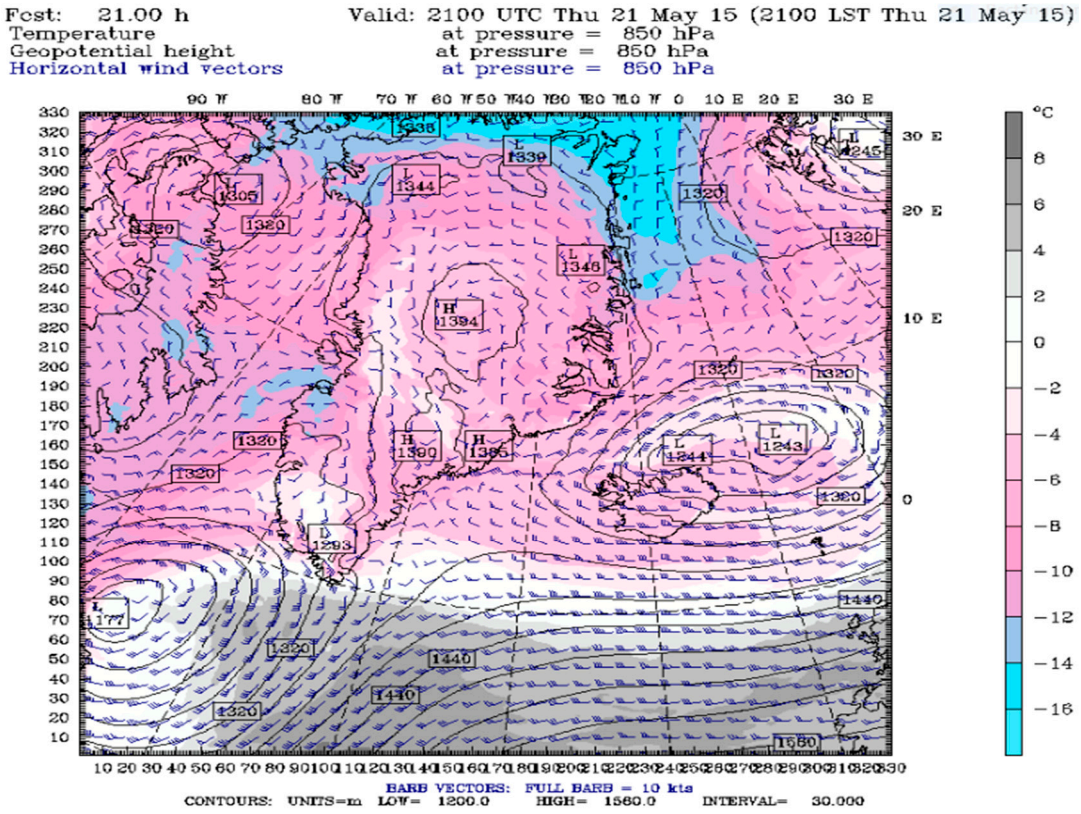

Figure 5. OSU Polar WRF 850 hPa forecast for 21Z on 21 May 2015.

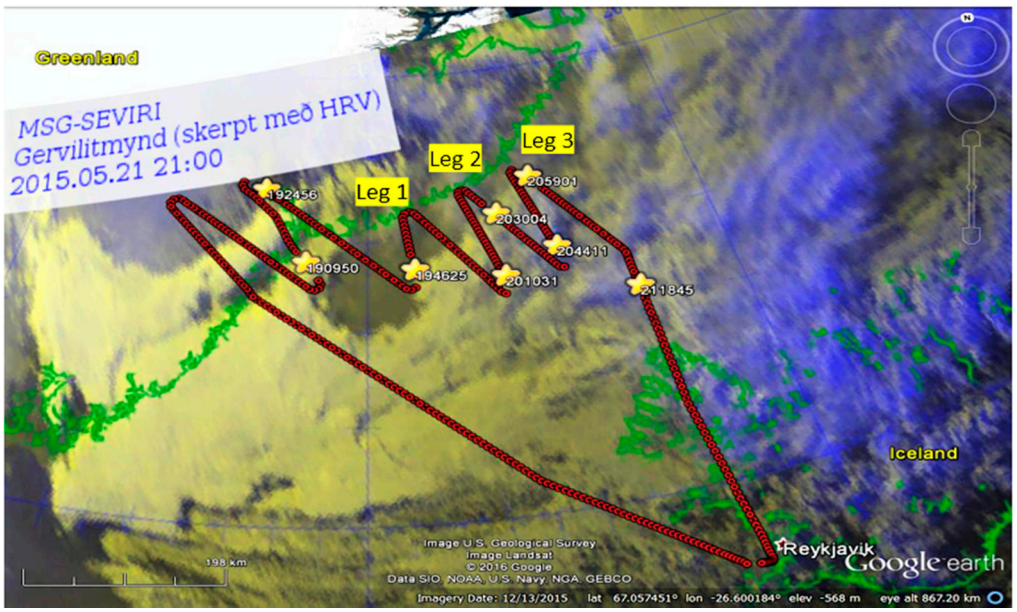

Figure 6. DC-8 Flight track, DAWN profile locations (red dot) and dropsonde locations (gold star) during the 21 May 2015 flight mission. Satellite imagery from MSG-SEVIRI (Data processed by the Icelandic Meteorological Office) at 21Z. Labels for NW–SE legs provided at the beginning of the leg (after the turn).

A detailed modeling study of this wind event and comparisons between the model forecasts and DAWN and dropsonde observations were also previously discussed by the authors [24]. For this case study, we analyze output from the same model used in that study. As discussed in Section 2, the parameterizations and settings of this version of the WRF model were determined through sensitivity tests of barrier wind simulations.

During this mission, DAWN profiles were attempted every 4 km with 23–29 possible profiles for each "leg" of the zig zag flight pattern shown in Figure 6. Figure 7 shows the DAWN wind speed and wind direction along three of the NW–SE legs flown off the coast in the area of the barrier winds. To limit the contamination by aircraft motion (roll), each leg began with the first good profile after the turn and ended with the last good profile before the turn or change in direction. As seen from satellite imagery in Figure 6, there were clouds present during the leg transects, which sometimes attenuated the signal to where it was too weak to determine a profile as indicated by the missing data in Figure 7. During Leg 1, the DC-8 was flying at an altitude of around 5.5 km but low level clouds prevented any profile information below 1.5–2 km. As a result, the aircraft descended to 2.5 km for the rest of the mission where full profiles were obtained over significant portions of the legs. Individual DAWN wind profiles are compared with co-located dropsondes and the WRF forecasts. These are shown for two locations close (~75 km) to the coast (Figures 8 and 9) and two locations 60–80 km further east (Figures 10 and 11). These figures show that the DAWN wind profiles closely match those as measured by the dropsonde. Both the individual dropsonde and DAWN profiles as well as the DAWN leg transects (Figure 7) show a weaker, narrower jet near the coast (~20 m/s around 500 m) but a deeper and stronger wind maximum further off the coast (24–26 m/s between 500 m and 1200 m) as well as a veering from NNW–N to NE–ENE between 1 and 2 km. Both of these features are consistent with previous findings [24,35].

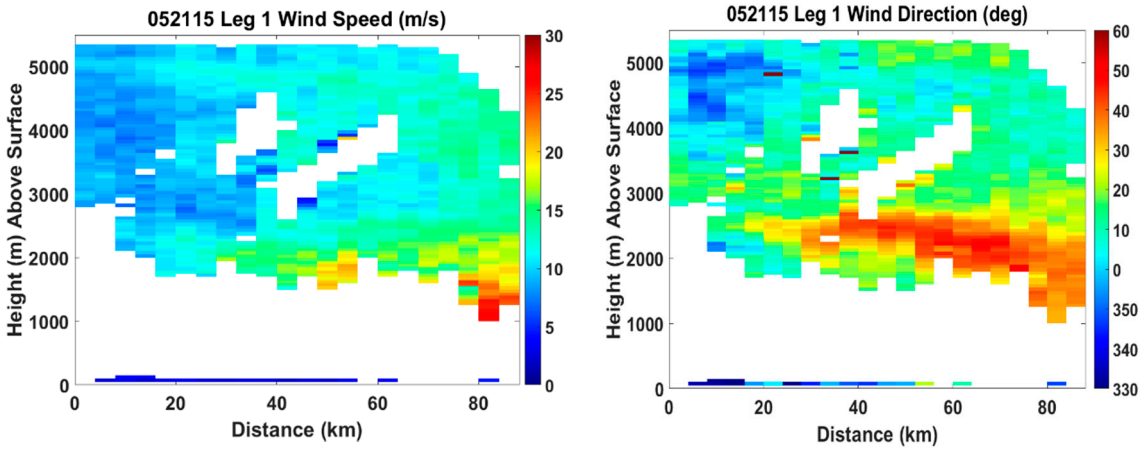

Figure 7. *Cont.*

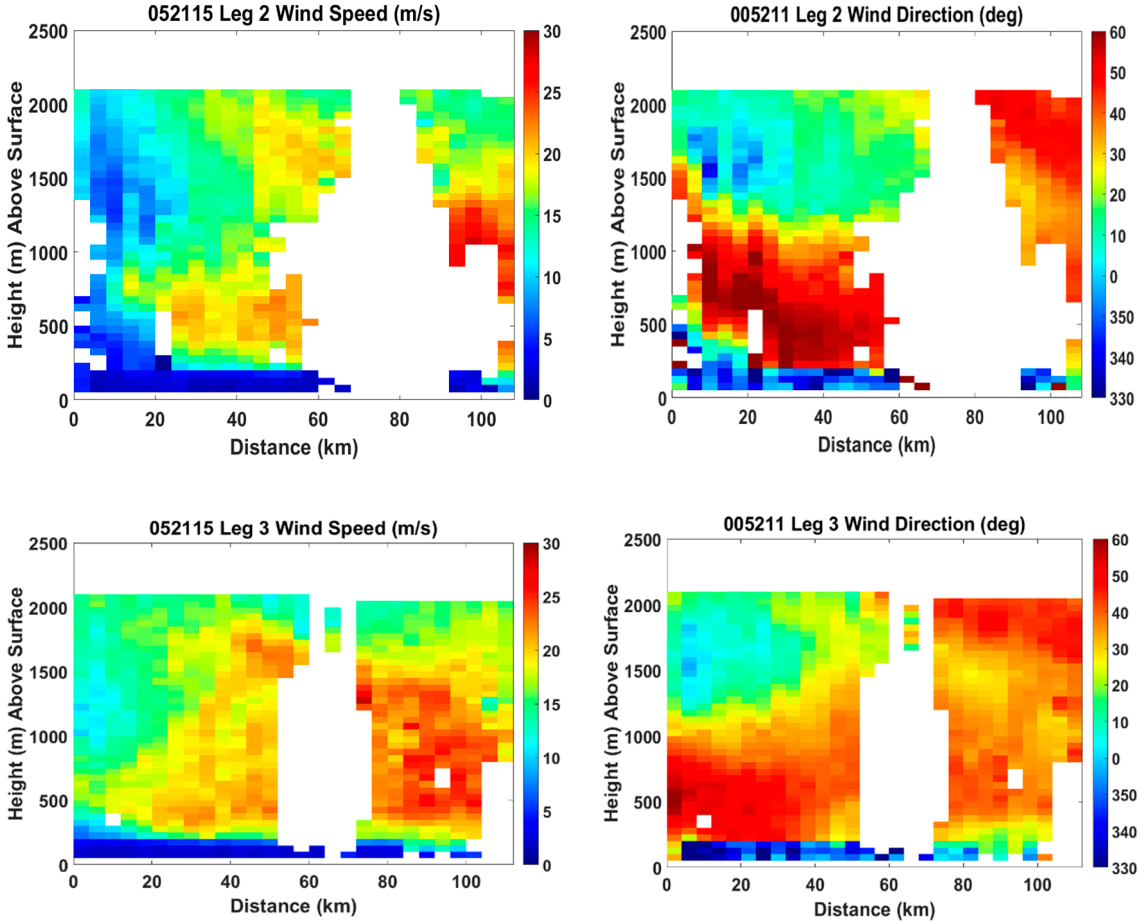

Figure 7. DAWN wind speed (**left**) and wind direction (**right**) cross section during the three NW–SE legs from turn to turn: Leg 1(**top**), Leg 2 (**middle**) and Leg 3 (**bottom**) on 21 May 2015.

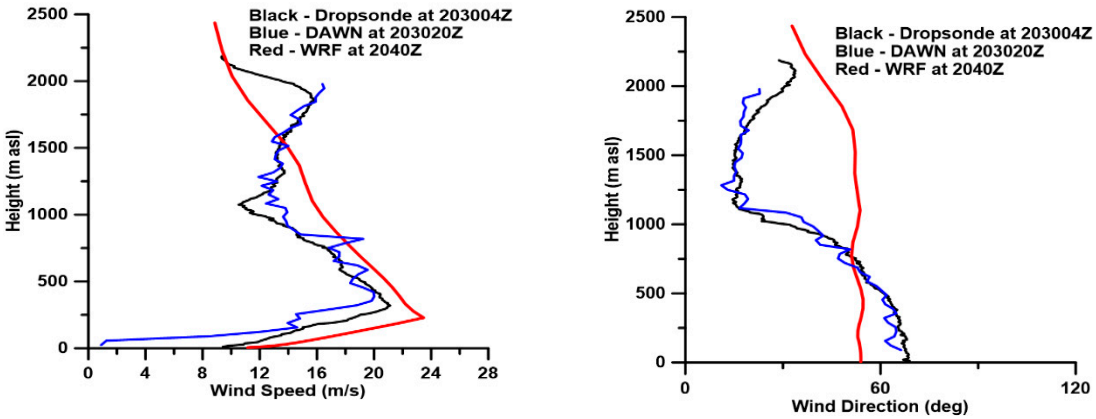

Figure 8. DAWN, dropsonde and model profiles of wind speed (**left**) and wind direction (**right**) closer to the coast around 2030Z on 21 May 2015.

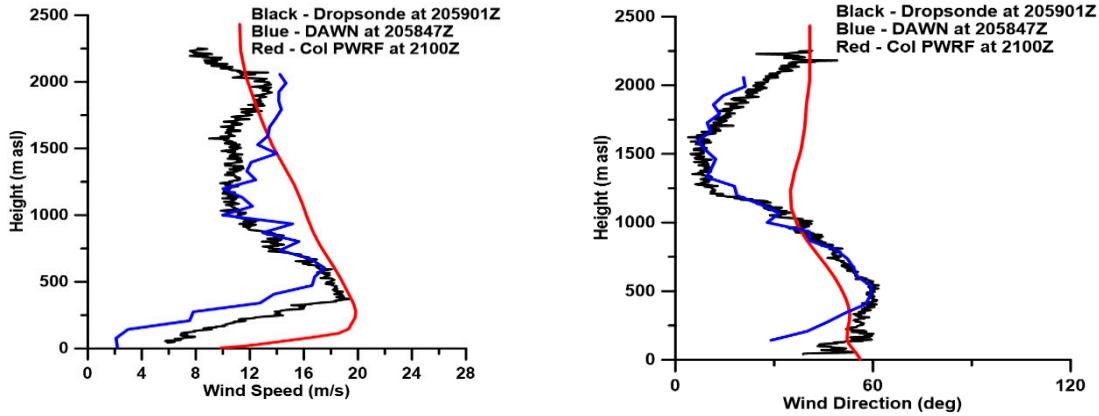

Figure 9. DAWN, dropsonde and model profiles of wind speed (**left**) and wind direction (**right**) closer to the coast around 2100Z on 21 May 2015.

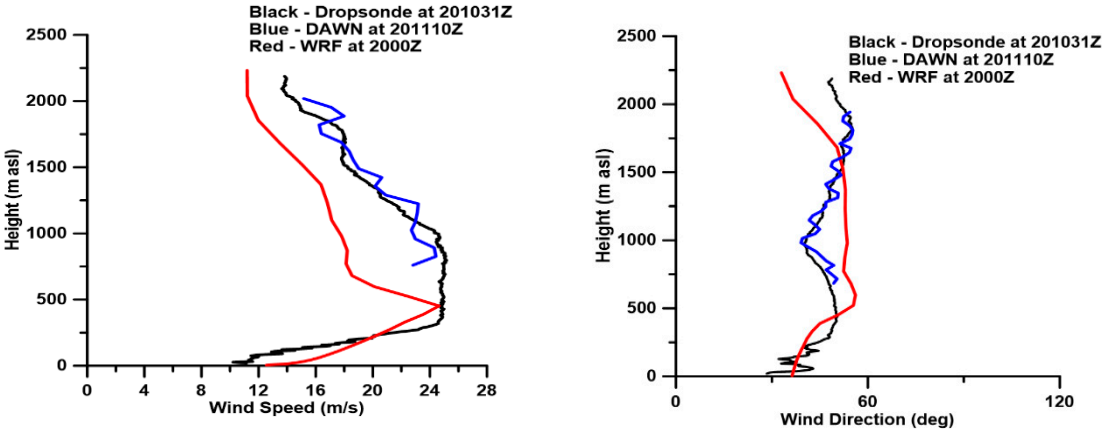

Figure 10. DAWN, dropsonde and model profiles of wind speed (**left**) and wind direction (**right**) further off-shore around 2010Z on 21 May 2015.

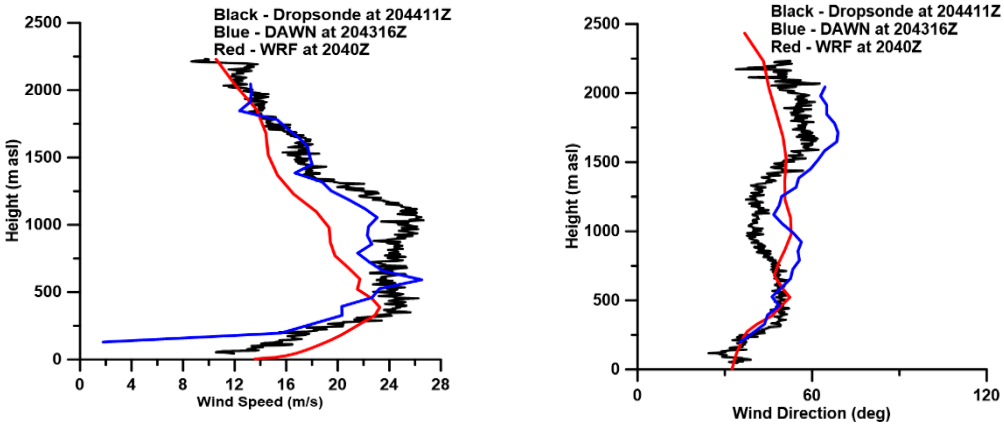

Figure 11. DAWN, dropsonde and model profiles of wind speed (**left**) and wind direction (**right**) further off-shore around 2041Z on 21 May 2015.

Comparisons between the DAWN and dropsondes with the model presented in Figures 8–11, as well as the comparisons at the other four dropsonde locations (two limited by incomplete DAWN profiles) not presented, show good agreement but with some differences. Closer to the coast, the model slightly over forecasts the speed of the jet and while it capture the directional changes in the bottom 500 m, it does not capture the variability in wind direction and the backing with height above that level

that is observed by DAWN and dropsondes. Further off the coast, the model does a good job forecasting the wind direction change with height throughout the bottom 2 km as well as the intensity of the jet, but not capturing the depth of the strong winds as shown by observations. These figures suggest the observations may be showing the characteristics of more mesoscale features—and possibly microscale features—than are being depicted in the simulations with coarser horizontal resolutions. A possible reason for the differences could be the presence of low-level clouds, as seen in Figure 6, as clouds are often linked with sharp gradients and transitions and are tied in dynamically and interactively with mixed-layers, inversions, cloud top cooling. The relative humidity profiles of both the model and dropsondes presented in Figure 12 show this difference/increase in humidity/clouds moving further offshore (also seen in Figure 6 satellite imagery) as well as the inability of the model to capture the variability of moisture in the vertical as observed by the dropsondes. The model also forecasted higher relative humidity further off the coast than what was observed by the dropsondes, which were launched during breaks in the clouds.

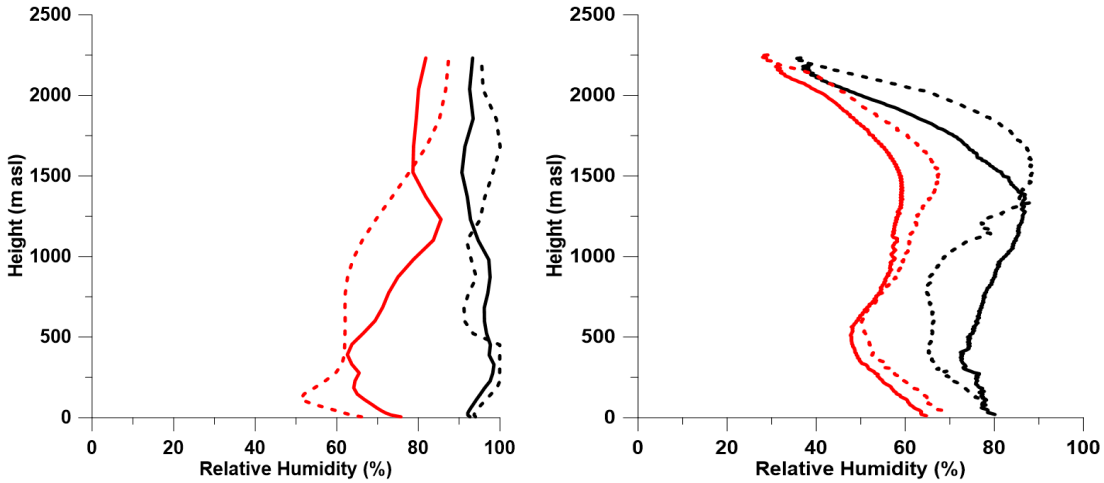

Figure 12. Model (**left**) and dropsonde (**right**) relative humidity profiles for closer to the coast at ~2033Z (red solid) and ~2059Z (red dash), and further off-shore at ~2011Z (black solid) and 2044Z (black dash) on 21 May 2015.

4.2.2. Greenland Tip Jet during PW1 on 31 October 2014

The region off of the southern tip of Greenland is noted as one of the windiest places on the planet for the lower levels of the atmosphere. This is the result of the low pressure systems crossing the Atlantic Ocean and the formation of the Greenland tip jet, which develops due to the prevailing low level flow around these circulations being impacted (accelerated) by the shape and terrain of the Greenland coastline. This tip jet, which may be easterly or westerly depending on the circulation, has been studied by many researchers [35,36,38–41]. Like the barrier winds, the tip jet has been the subject of previous field campaigns such as GFDex [4] and ADWL investigations [3,13].

The most common time of the year for these events are the winter season, unfortunately between the two Polar Winds campaigns of 2014 and 2015. However, fortunately there was a weak easterly tip jet on 31 October 2014, likely connected to low level barrier winds along the south east coast of Greenland. The ECMWF 12Z analysis of the wind field at 925 hpa (~750 m) presented in Figure 13 shows a low pressure system south of Iceland and both a barrier wind event on the east coast of Greenland and a weak easterly tip jet event. Figure 13 also provides MSG-SEVIRI Infrared imagery which shows mostly clear conditions off the tip of Greenland but perhaps some low level clouds. The flight track of this mission is shown in Figure 14 and targeted the region just east and south of Cape Farewell and the tip of Greenland to capture the southern end of the barrier wind and the weak acceleration around the tip of Greenland. Seven flight "legs" are identified for the discussion of this

part of the mission. During these legs, the NASA King Air aircraft was flying between 1.8 km and 2 km to get below a deck of clouds and attempted DAWN profiles every ~5 km.

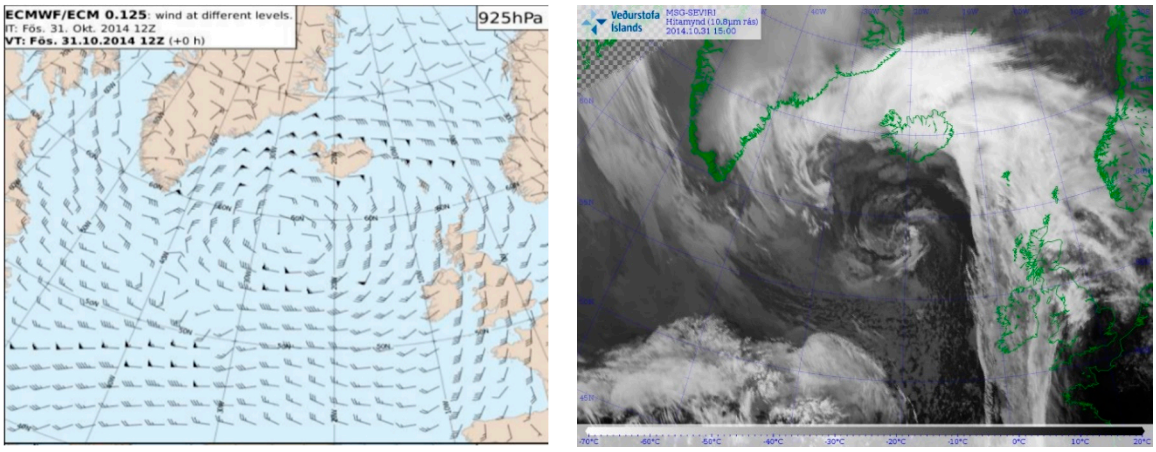

Figure 13. ECMWF low-level wind field (925 hPa/~750 m) ANALYSIS (00 hr forecast) on 12Z 31 October 2014 (**left**) and MSG-SEVIRI IR satellite imagery at 15Z (**right**) when the DC-8 was just off the tip of Greenland (Images and Data processed by the Icelandic Meteorological Office).

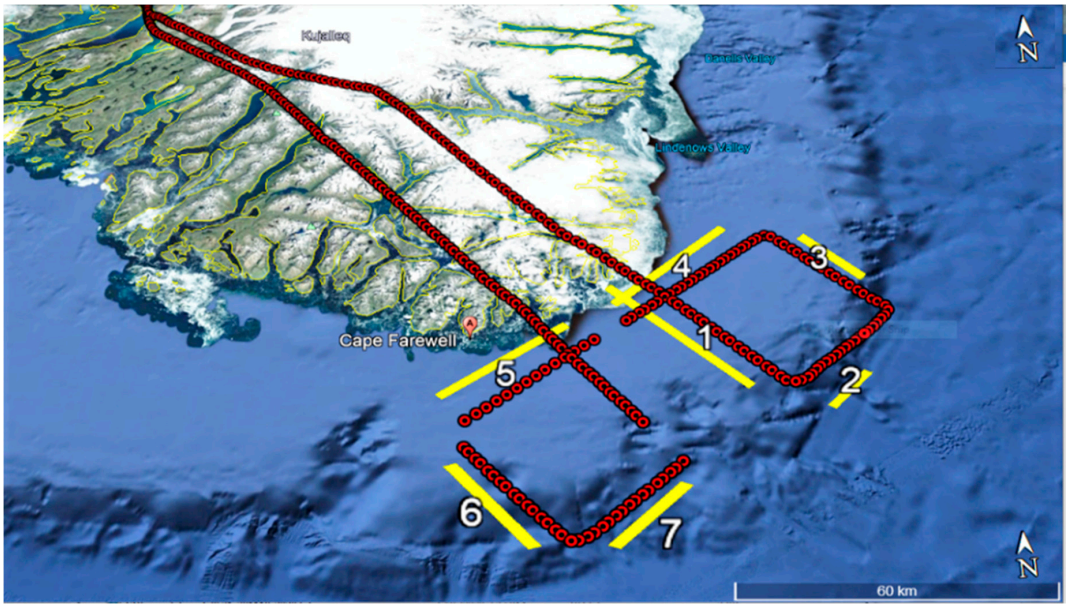

Figure 14. Flight track and DAWN profile locations (red dot) during the 31 October 2014 flight mission with identified flight legs 1–7 (Google Earth).

As mentioned above, there were issues with the aerosol sensitivity of DAWN during the field campaigns and, as a result, DAWN had a difficult time obtaining a sufficient signal when the aerosol concentration was very low. Even flying at 2 km, this was the case on 31st October, but mainly for above 1.4 km with the exception being a low aerosol layer (from SNR) between 1.1 and 1.2 km. Below that level, low-level aerosols, including those from sea spray, enabled continuous measurement of the boundary layer in certain segments. Thus, this allowed us to measure up to or at least close to the level where the maximum of the tip jets are usually found.

Figure 15 provides examples of the DAWN vertical profiles (wind speed and direction, LOS SNR) in leg 3 just east of the tip of Greenland and in leg 6 further west and south of the tip. These profiles clearly show the stronger winds associated with the southern edge of the barrier winds and the weak jet around the tip above 75–100 m. Below this level, the decrease in wind speeds and the backing of the

wind direction closer to the surface is an artifact of the DAWN data processing that arises due to the leading edge of the Gaussian lidar pulse going below the surface. Recent work has been successful in developing processing algorithms to obtain more information in the 0–25 m above ground level layer and spray zone [42]. One other feature of Figure 14 that needs noting is that in leg 6 above 1 km where, despite the weak SNR (lack of aerosols), some bad data points passed the processing GOF threshold mentioned in Section 3.2.

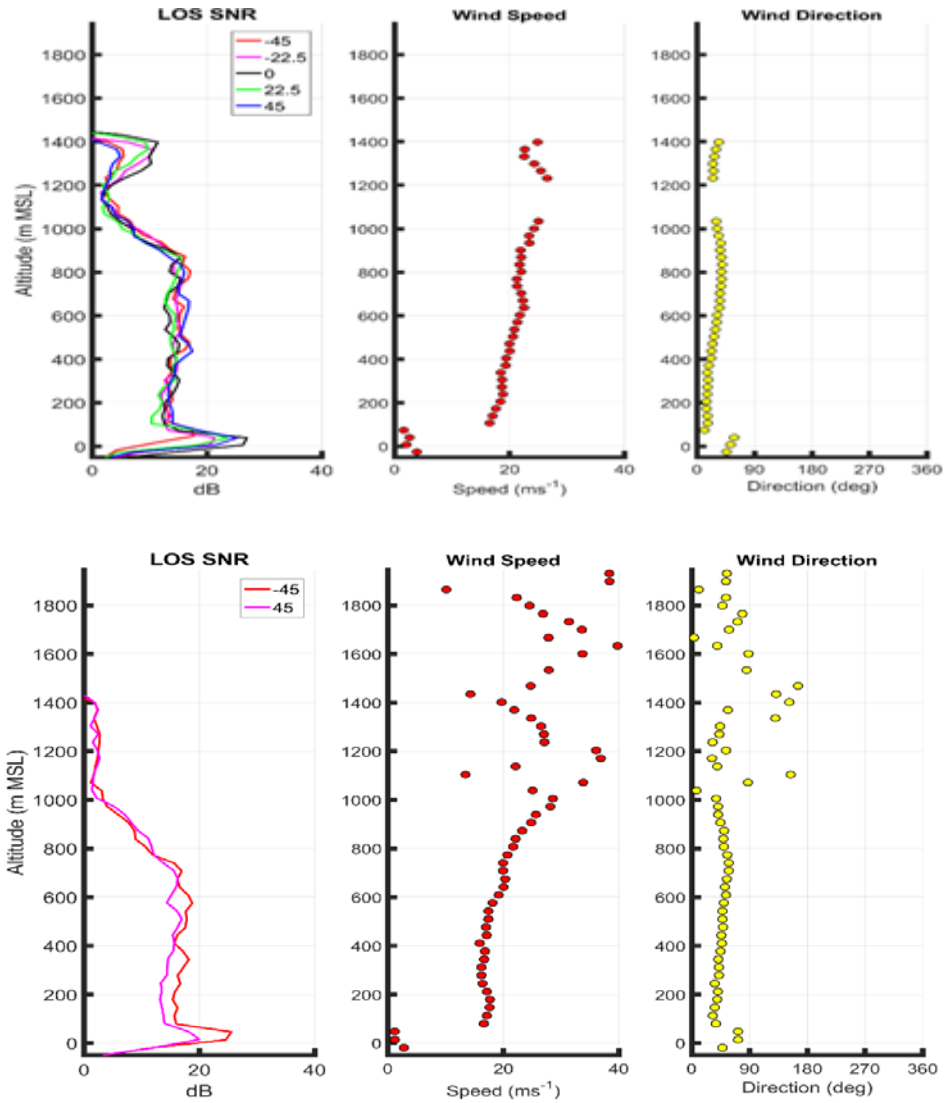

Figure 15. DAWN vertical profiles of LOS SNR, wind speed and wind direction east of the tip in leg 3 (**top**) and south of the tip in leg 6 (**bottom**) on 31 October 2014 around 1530Z.

Figure 16 provides an x–z cross section of wind speed and direction along the NW–SE oriented legs from 3 (east of the tip) to 1 and 7 (south of the tip and Cape Farewell) while Figure 17 provides similar cross sections for combined legs 4 and 5 just south of the tip moving east to west. From these figures, we can see that the maximum of the jet is somewhere near 900–1100 m and increases east to west further away from the tip but decreases east to west (legs 4–5) closer to the tip. The veering of the wind direction from northerly to more easterly is also clearly seen in as the aircraft moves from east of the tip to west of the tip. Both Figures 16 and 17 omit data for below 100–150 m. This is done because, while the returns from below this level show high SNR, which is indicative of high backscatter from sprays and probably foam given the high winds, the computed values for the winds are questionable.

This is due to the size (75 m) of the sliding range gate used and the shape of the monitor pulse as it nears the surface. Current work is focused on retrieving profile data in the bottom 50 m of the profile.

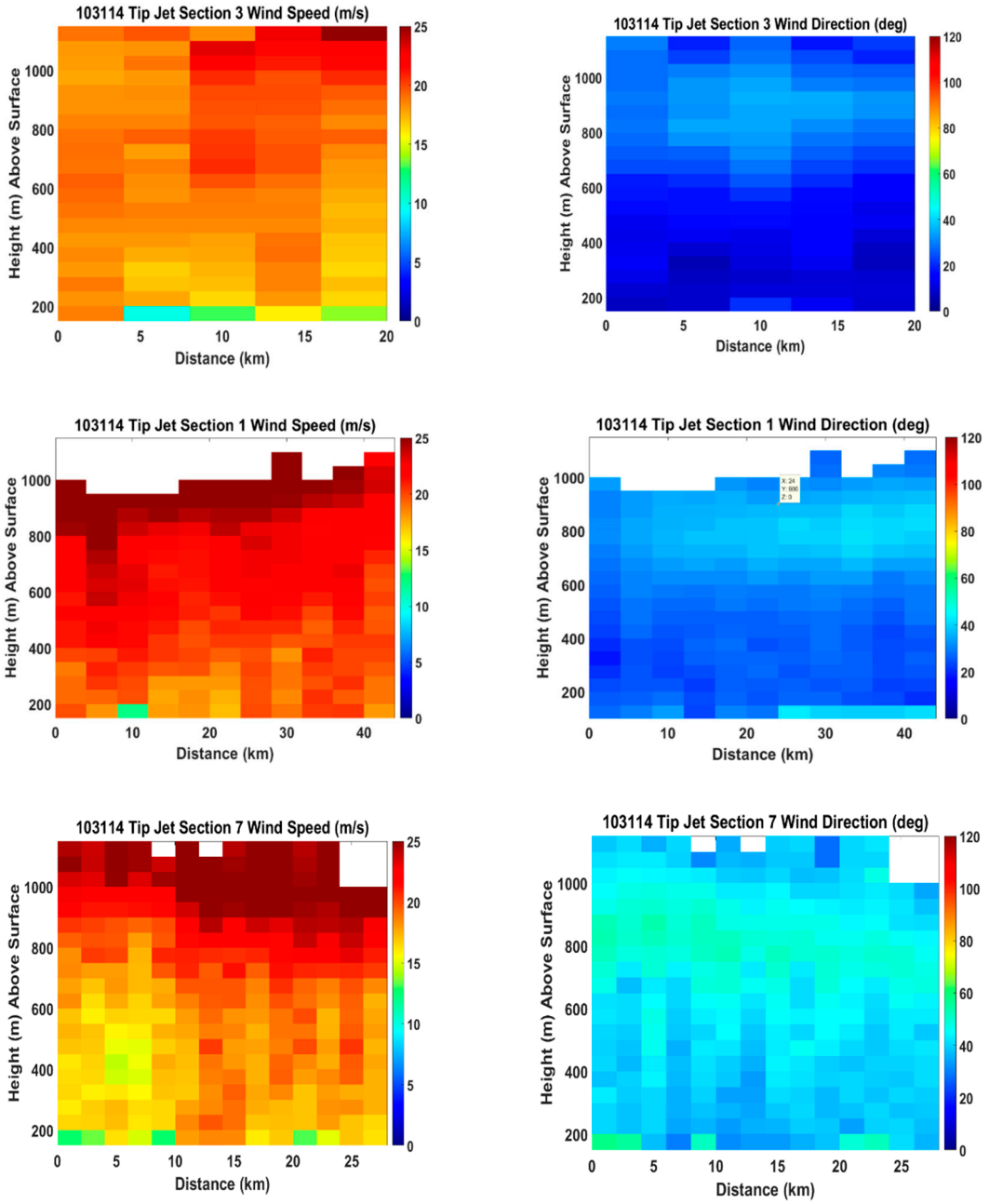

Figure 16. x–z cross section of DAWN wind speed (**left**) and direction (**right**) along the NW–SE oriented legs from 3—east of the tip (**top**) to 1—south of the tip (**middle**) and 7—south of Cape Farewell (**bottom**) on 31 October 2014.

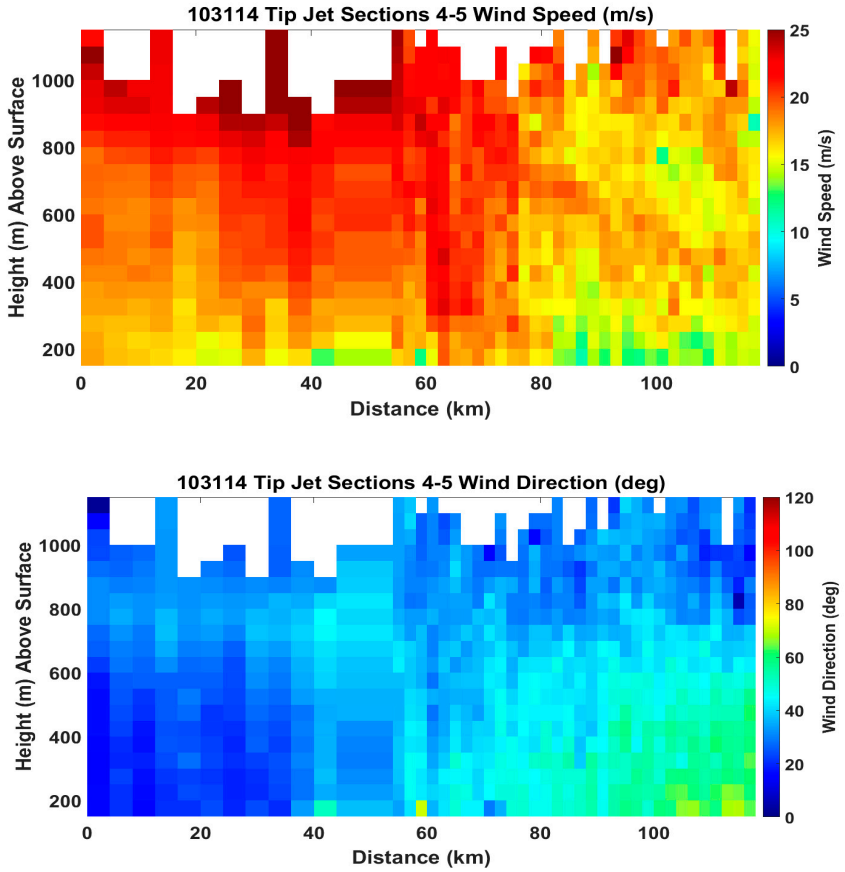

Figure 17. x–z cross section of DAWN wind speed (**top**) and direction (**bottom**) for combined segments 4 and 5 just south of the tip moving east to west on 31 October 2014.

Although no dropsondes were used during PW1, comparisons between the observed DAWN profiles and those forecasted by the operational Polar WRF detailed in Section 2 were still possible. Examples of the comparisons between the near complete DAWN profile winds and the winds forecasted by the Polar WRF at the closest model grid point are presented. Comparisons for east of the tip and at the southern edge of the barrier winds at the beginning of leg 1 and the middle of leg 3 shown in Figure 13 are displayed, respectively, in Figures 18 and 19. From these figures, we can see that the operational Polar WRF does a good job in forecasting the wind speeds in this area up to around 800 m but does not do as good of a job in capturing the changing of the wind direction (veering to a more easterly component) from east (leg 3) to west (leg 1) below 7–800 m. Further west, the DAWN-model comparisons south of the tip presented for the middle of leg 6 (Figure 20) and leg 7 (Figure 21) show that the model does a good job in capturing the observed wind speeds below 600 m, but significantly underestimates the accelerations above this 600–800 m level. As seen from the model temperature and water vapor mixing ratio profiles shown in Figure 22, it is right around 600 m where the model shows both a small inversion and significant change (decrease) in moisture above that level both east and south of the tip. These moisture and temperature changes in the vertical and at that level may lead to the inability of the model to resolve the low-level static stability profile and leading to the differences seen in the wind profile. In addition, the model does not forecast the observed continued veering of the wind to a more ENE (60 degrees) direction close to the tip but handles the smaller veering further off the tip in leg 7. From these comparisons, it is evident that boundary layer scheme chosen for the operational Polar WRF results is very smooth and unchanging winds over significant layers and does not capture the variability in the DAWN profiles in the lower levels. This must be taken into consideration in future operational modeling of these events.

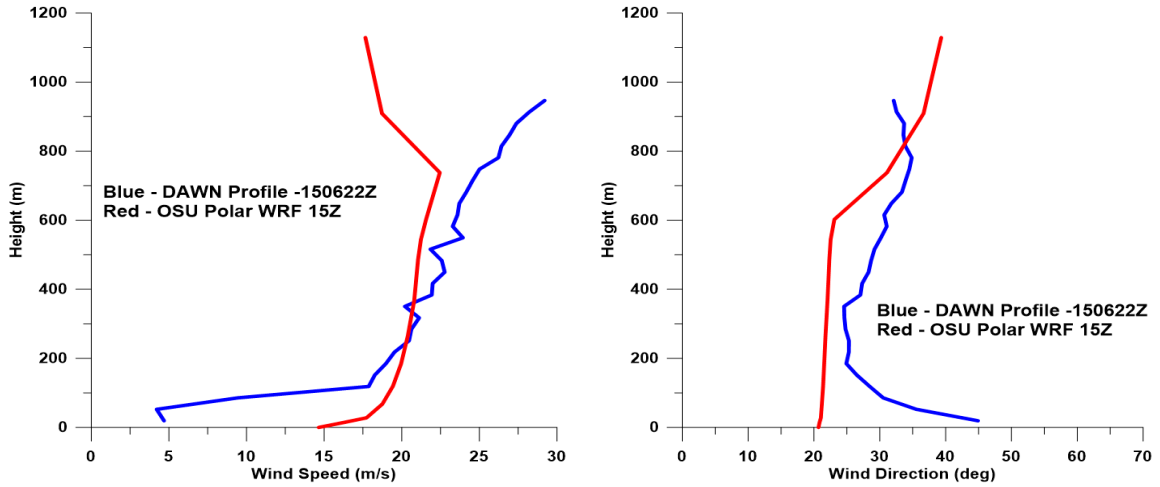

Figure 18. DAWN and model profiles of wind speed (**left**) and wind direction (**right**) near 1506Z on 31 October 2014 for the beginning of leg 1 east of the tip.

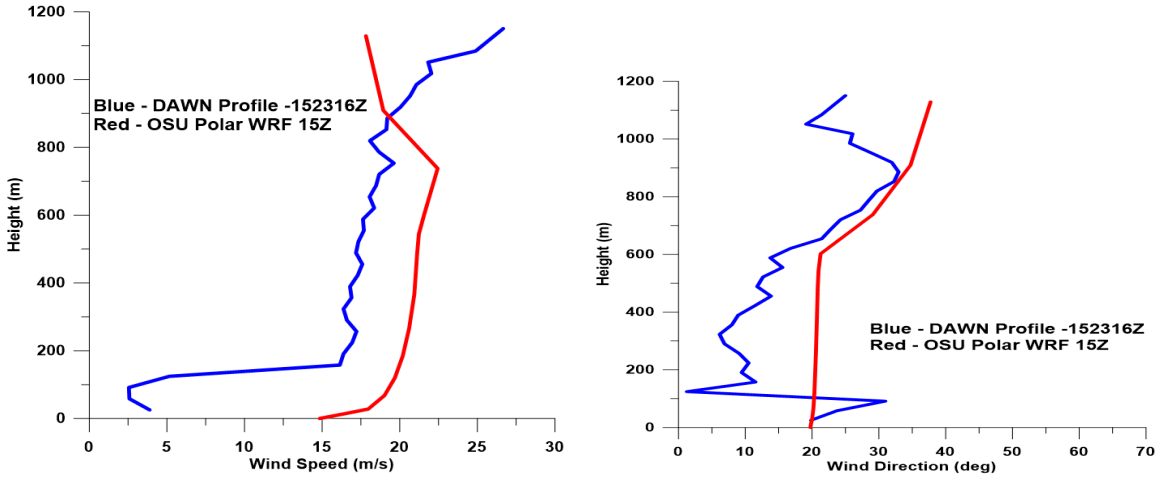

Figure 19. DAWN and model profiles of wind speed (**left**) and wind direction (**right**) near 1523Z on 31 October 2014 for the middle of leg 3 east of the tip.

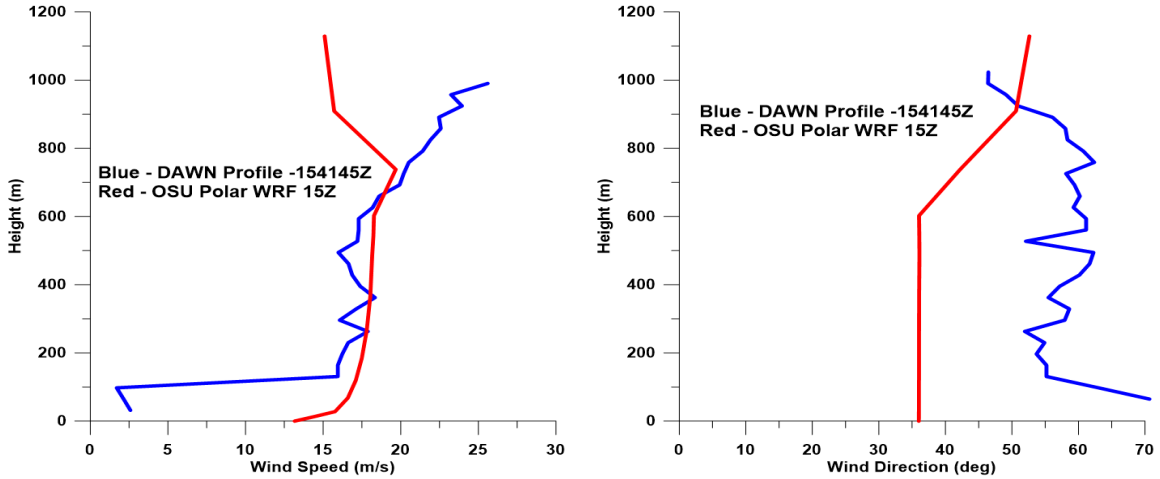

Figure 20. DAWN and model profiles of wind speed (**left**) and wind direction (**right**) near 1542Z on 31 October 2014 for the middle of leg 6 south of the tip.

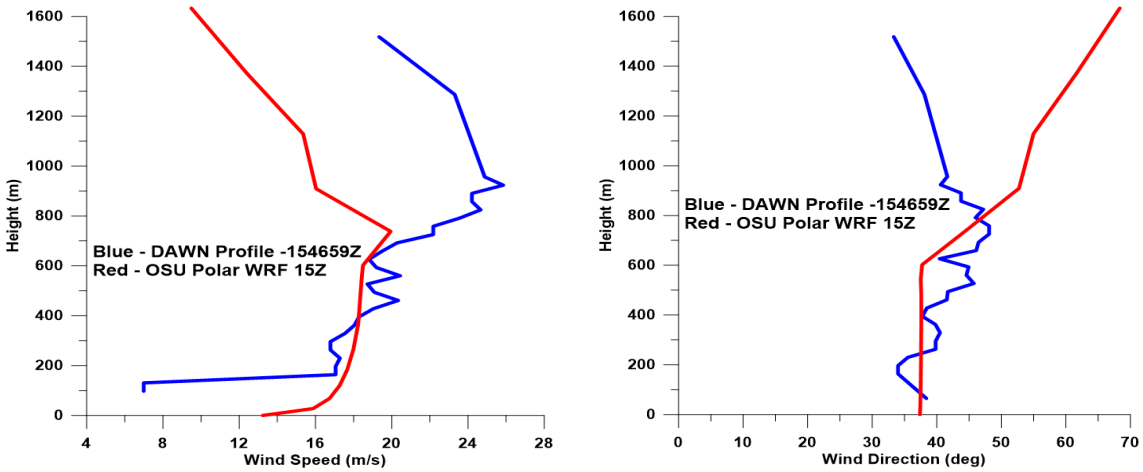

Figure 21. DAWN and model profiles of wind speed (**left**) and wind direction (**right**) near 1523Z on 31 October 2014 for the beginning of leg 7 south of the tip.

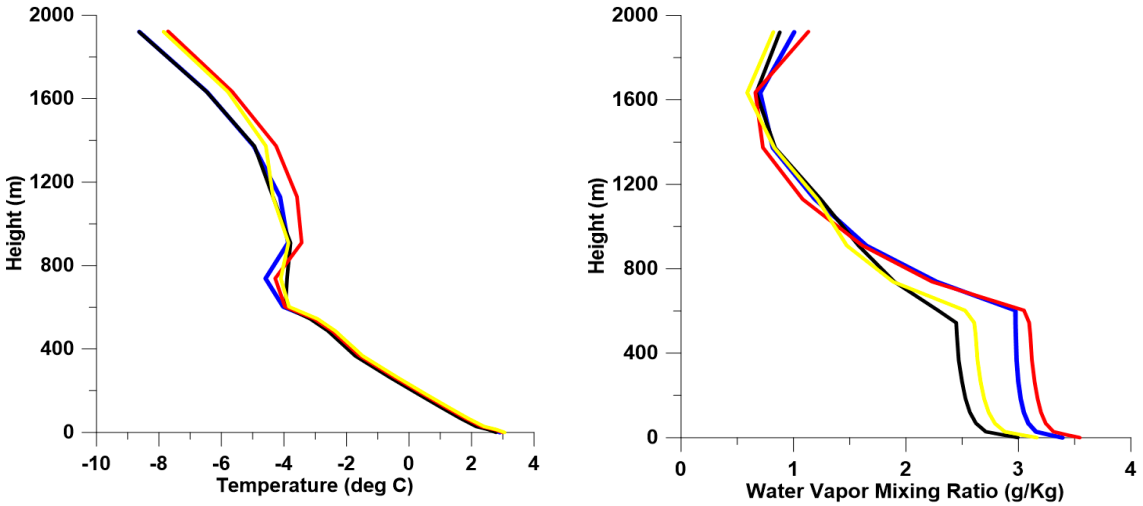

Figure 22. Polar WRF profiles of temperature (**left**) and water vapor mixing ratio (**right**) in leg 3 (red), leg 4 (yellow), leg 6 (black) and leg 7 (blue). The gradient from north to south is also clearly seen.

4.2.3. Upper Level Jet during PW2 on 19 May 2015

In addition to investigating the low-level circulations of the Arctic, Polar Winds missions were also flown to study the strong upper level jets and upper air cyclones of the region. One such investigation took place along the southeastern coast of Greenland on 19 May 2015. The upper jet across the tip and along the coast can be seen in Figure 23 with the flight path along the coast from north to south, and the location of dropsondes, are shown in Figure 24.

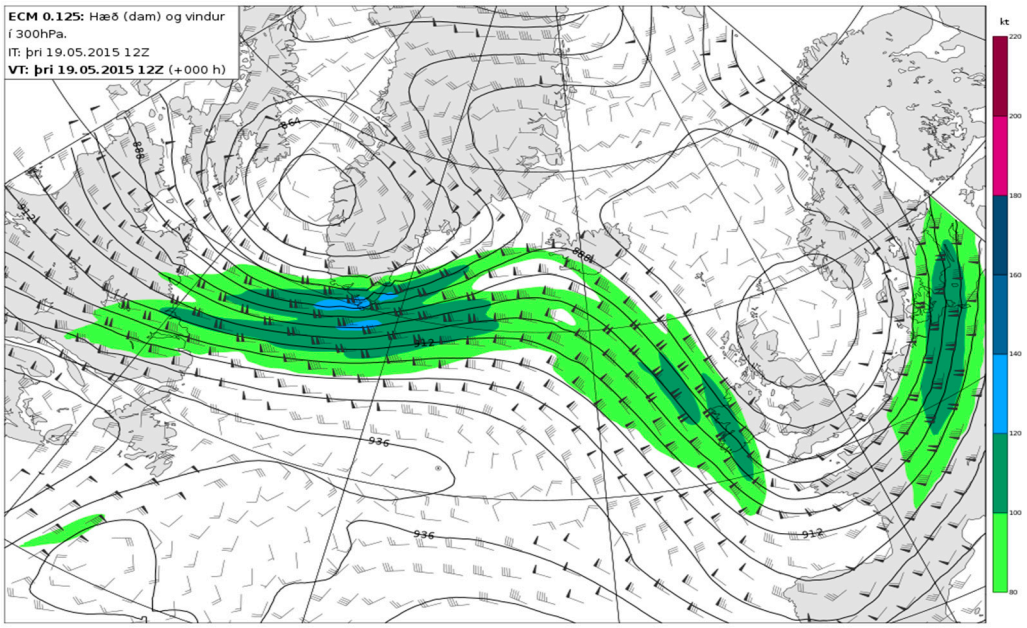

Figure 23. ECMWF 0-hr analysis for upper winds (300 hPa/~9.1 km) on 12Z 19 May 2015. (Data processed by the Icelandic Meteorological Office).

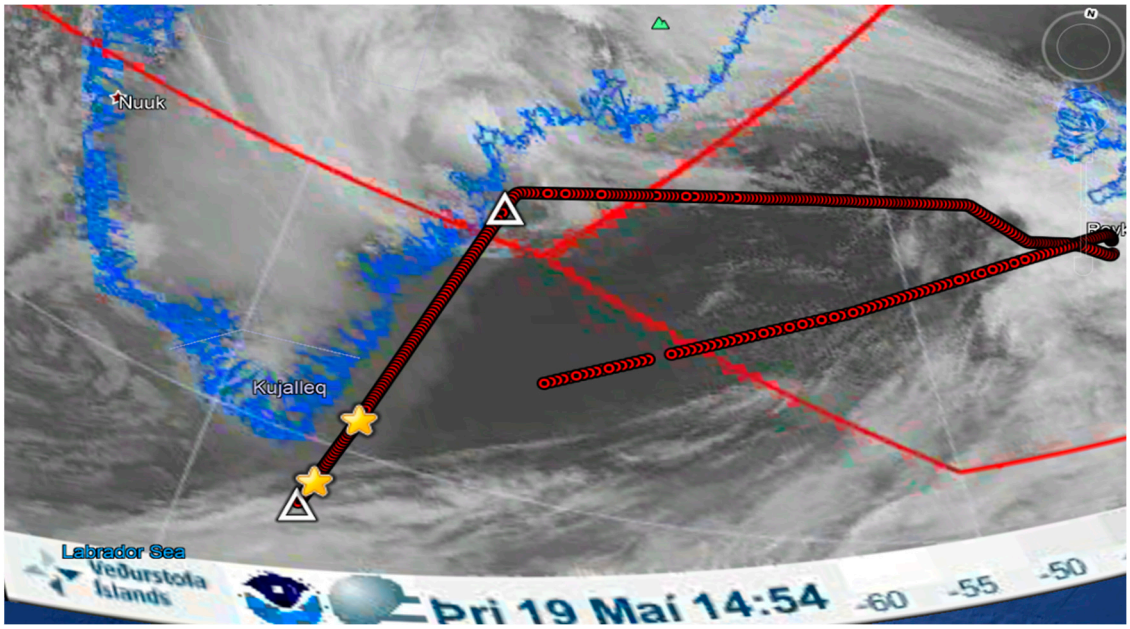

Figure 24. Flight track and DAWN profile locations (red dot) and dropsonde locations (gold star) during the 19 May 2015 flight mission. Start and end of leg used for cross-section denoted by white triangle. IR satellite imagery from MSG-SEVIRI near15Z (Google Earth). Image processed by the Icelandic Meteorological Office.

One hundred DAWN profiles over approximately 500 km (~5 km horizontal spacing) were taken along the coastal leg going north to south. Unfortunately, the atmosphere in the lower and mid-levels were very clean and free of aerosols along this leg, thus preventing wind measurements at these levels. However, the DAWN was able to take coherent and complete measurements in the 1–2 km below the aircraft flight level and able to capture much of the upper jet over the entire leg. The north–south vertical cross-sections in the 6–8 km altitude range for wind speed and wind direction are shown in Figure 25. The high resolution variations in both wind speed and wind direction are clearly evident

from the DAWN measurements, as are the increased intensity and depth in the upper jet near the tip of Greenland.

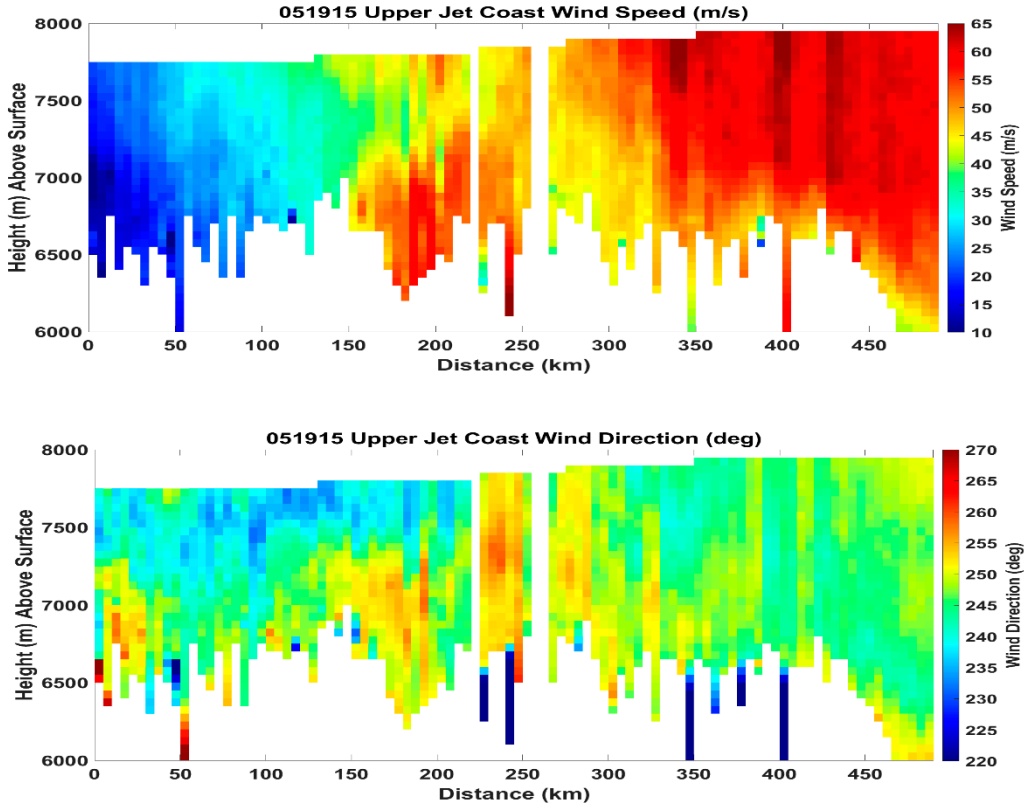

Figure 25. North–south x–z cross section of DAWN wind speed (**top**) and direction (**bottom**) for coastal flight segment off the east coast of Greenland on 19 May 2015.

The comparison between the dropsondes and the closest DAWN profiles are shown in Figures 26 and 27. Once again, the very close similarity in wind speed and wind direction between the DAWN profiles and the more historic and trusted dropsondes helps validate the use of the DAWN profiles for studying features and conducting future model validation in the Arctic.

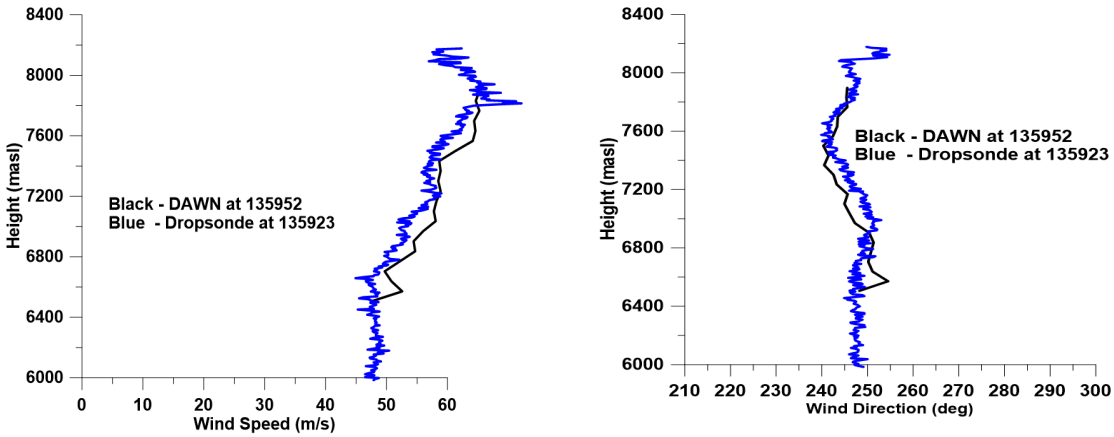

Figure 26. DAWN and dropsonde profiles of wind speed (**left**) and wind direction (**right**) around 1359Z on 19 May 2015.

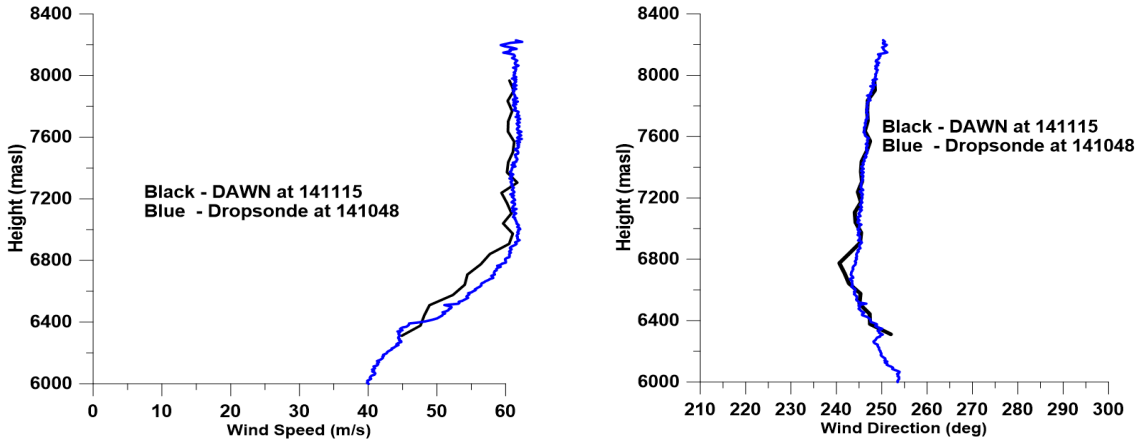

Figure 27. DAWN and dropsonde profiles of wind speed (**left**) and wind direction (**right**) around 1411Z on 19 May 2015.

5. Discussion

As discussed above, the DAWN instrument faced backscatter sensitivity issues, particularly in low aerosol conditions that were fairly frequent in the 2–6 km altitude range. However, since the completion of Polar Winds, the following changes have been made to DAWN:

- Pulse Repetition Frequency increased from 5 Hz to 10 Hz;
- Repairs to optical path (alignments, fiber connections);
- Scanner look angle options increased to include 8 and 12 looks;
- DAWN enclosure modified to allow easier access to the lidar during deployment.

The improved DAWN instrument was flown during NASA's 2017 CPEX over the Gulf of Mexico and Caribbean Sea and the 2019 Aeolus Cal/Val preparatory campaign in the northeastern Pacific Ocean. Results from these experiments have shown that these modifications have helped improve the sensitivity of DAWN in the processing of the raw lidar data and enabled fuller vertical wind profiles in the presence of weaker aerosols, which often occurs over tropical oceans as well as in the arctic regions near Greenland.

6. Conclusions

During October–November 2014 and May 2015, NASA conducted two airborne field campaigns, collectively called Polar Winds, to fly an airborne Doppler wind lidar called DAWN to take airborne wind and aerosol measurements of the Arctic atmosphere and PBL over the Polar seas and ocean. Between the two campaigns, over 100 flight hours of DAWN were flown and, during PW2, almost 100 dropsondes were also launched to provide truth or validation

Comparisons between wind profiles taken from DAWN and those from the more traditional dropsondes show very good agreement and very low bias. This is true despite time and location differences in the measurement volume between dropsondes and the DAWN pulsed lidar and supports the use of an airborne Doppler wind lidar such as DAWN to provide wind profiles that have high velocity precision, ~65 m vertical resolution and horizontal spacing as fine as 3–7 km.

Individual case studies were presented and, despite some of the issues with the DAWN sensitivity, the wind profiles generated by DAWN are very promising with regard to both diagnostic studies of dynamic features such as upper level and low-level jets (tip jet and barrier winds) and for utilization in model validation.

Author Contributions: G.D.E. and M.K. oversaw the deployment of DAWN for the Polar Winds Field campaigns with M.K. as the Instrument PI and G.D.E. acting as the Science PI for DAWN. G.D.E. and S.G. participated in the Polar Winds field campaigns, provided meteorological support and conducted quick-look processing of

DAWN data. S.G. and G.D.E. were responsible for software development and final data processing of DAWN data. K.H. and A.D. tuned the WRF model for operational (K.H.) and post-campaign research (A.D.). S.G. and G.D.E. conducted the comparisons between DAWN and dropsondes, while all authors were involved in the DAWN-model comparison. S.G. and G.D.E. were the primary authors of the manuscript but all authors contributed to the discussion and analysis of the results and refinement of the paper. All authors have read and agreed to the published version of the manuscript.

Funding: This research was funded by the United States National Aeronautics and Space Administration (NASA) under contracts NNL14AA14C and NNX17LB41P.

Acknowledgments: We would like to thank the Earth Science Division of NASA's Science Mission Directorate for organizing and conducting Polar Winds, the Earth Science Technology Office (ESTO) for sponsoring the DAWN lidar, and would especially like to acknowledge the NASA LaRC Engineering Directorate for providing and operating DAWN during Polar Winds. We would also like to thank Mark Beaubien of YES for help with the dropsonde data and processing.

Conflicts of Interest: The authors declare no conflict of interest.

Abbreviations

The following abbreviations are used in this manuscript:

ADWL	Airborne Doppler Wind Lidar
ALADIN	Atmospheric Laser Doppler Instrument
ASCAT	Advanced Scatterometer
ASR	Arctic System Reanalysis
CALIPSO	Cloud-Aerosol Lidar and Infrared Pathfinder Satellite Observations
CPEX	Convective Processes Experiment
DAWN	Doppler Aerosol WiNd Lidar
DC-8	Douglas Craft-8
DLR	German Aerospace Research Establishment Deutsches Zentrum für Luft- und Raumfahrt
ECMWF	European Centre for Medium-Range Weather Forecasts
ERA	ECMWF Re-Analysis
FFT	Fast Fourier Transform
FWHM	Full Width Half Max
GFDex	Greenland Flow Distortion Experiment
GFS	Global Forecast System
GOES	Geostationary Operational Environmental Satellite
GOF	Goodness of Fit
GPS	Global Positioning System
GRIP	Genesis And Rapid Intensification Processes
HDSS	High Definition Sounding System
HLOS	Horizontal Line-of-Sight
HoTmLiLiF	Holmium Thulium Lutetium Lithium Fluoride
InGaAs	Indium Gallium Arsenide
INS	Inertial Navigation System
IPY	International Polar Year
LaRC	Langley Research Center
LM	Levenberg–Marquardt
LOS	Line-of-Sight
METEOSAT	Meteorological Satellite
MODIS	Moderate Resolution Imaging Spectroradiometer
MOSAiC	Multidisciplinary Drifting Observatory for the Study of Arctic Climate
MM5	Fifth-Generation Penn State/NCAR Mesoscale Model
MSG	Meteosat Second Generation
MYJ	Mellor, Yamada, and Janjic
NASA	National Aeronautics and Space Administration
NCEP	National Center for Environmental Prediction
NOAA	National Oceanic and Atmospheric Administration
OSU	Ohio State University

PBL	Planetary Boundary Layer
P3DWL	P-3 Doppler Wind Lidar
PW1	Polar Winds 1
PW2	Polar Winds 2
RMSD	Root Mean Square Difference
RRTMG	Rapid Radiative Transfer Model for GCM
SEVIRI	Spinning Enhanced Visible and Infrared Imager
SNR	Signal to Noise Ratio
TCI	Tropical Cyclone Intensity
THORPEX	The Observing System. Research and Predictability Experiment
TODWL	Twin Otter Doppler Wind Lidar
UC-12	Utility Cargo-12
UW	University of Washington
WD	Wind Direction
WMO	World Meteorological Organization
WRF	Weather Research Forecast Model
WS	Wind Speed
WWRP	World Weather Research Program
XDD	eXpendable Digital Dropsonde
YES	Yankee Environmental Services
YOPP	Year of Polar Prediction
ΔWS	Wind Speed difference
ΔWD	Wind Direction
ΔZ	Height/altitude difference

References

1. Blunden, J.; Arndt, D.S. State of the Climate in 2019. *Bull. Am. Meteorol. Soc.* **2020**, *101*, Si–S429. [CrossRef]
2. Achtert, P.; Brooks, I.M.; Brooks, B.J.; Moat, B.I.; Prytherch, J.; Persson, P.O.G.; Tjernström, M. Measurement of wind profiles over the Arctic Ocean from ship-borne Doppler lidar. *Atmos. Meas. Tech.* **2015**, *8*, 4993–5007. [CrossRef]
3. Weissmann, M.; Busen, R.; Dörnbrack, A.; Rahm, S.; Reitebuch, O. Targeted observations with an airborne wind lidar. *J. Atmos. Ocean. Technol.* **2005**, *22*, 1706–1719. [CrossRef]
4. Renfrew, I.A.; Petersen, G.N.; Outten, S.; Sproson, D.; Moore, G.W.K.; Hay, C.; Ohigashi, T.; Zhang, S.; Kristjánsson, J.E.; Føre, I.; et al. The Greenland flow distortion experiment. *Bull. Am. Meteorol. Soc.* **2008**, *89*, 1307–1324. [CrossRef]
5. Kristjánsson, J.E.; Barstad, I.; Aspelien, T.; Føre, I.; Godøy, Ø.; Hov, Ø.; Irvine, E.; Iversen, T.; Kolstad, E.; Nordeng, T.E.; et al. The Norwegian IPY–THORPEX: Polar lows and Arctic fronts during the 2008 Andøya campaign. *Bull. Am. Meteorol. Soc.* **2011**, *92*, 1443–1466. [CrossRef]
6. Wagner, J.S.; Gohm, A.; Dornbrack, A.; Schafler, A. The mesoscale structure of a polar low: Airborne lidar measurements and simulations. *Q. J. R. Meteorol. Soc.* **2011**, *137*, 1516–1531. [CrossRef]
7. Marksteiner, U.; Reitebuch, O.; Rahm, S.; Nikolaus, I.; Lemmerz, C.; Witschas, B. Airborne direct-detection and coherent wind lidar measurements along the east coast of Greenland in 2009 supporting ESA's Aeolus mission. In *Lidar Technologies, Techniques and Measurements for Atmospheric Remote Sensing VII*; International Society for Optics and Photonics: Wales, UK, 2011; Volume 8182, p. 81820.
8. Marksteiner, U.; Reitebuch, O.; Lemmerz, C.; Lux, O.; Rahm, S.; Witschas, B.; Schäfler, A.; Emmitt, D.; Greco, S.; Kavaya, M.J.; et al. Airborne direct-detection and coherent wind lidar measurements over the North Atlantic in 2015 supporting ESA's aeolus mission. In *EPJ Web Conferences*; EDP Sciences: Les Ulis, France, 2018; Volume 176, p. 02011.
9. Marksteiner, U.; Lemmerz, C.; Lux, O.; Rahm, S.; Schäfler, A.; Witschas, B.; Reitebuch, O. Calibrations and wind observations of an airborne direct-detection wind LiDAR supporting ESA's Aeolus mission. *Remote Sens.* **2018**, *10*, 2056. [CrossRef]

10. Lux, O.; Lemmerz, C.; Weiler, F.; Marksteiner, U.; Witschas, B.; Rahm, S.; Schäfler, A.; Reitebuch, O. Airborne wind lidar observations over the North Atlantic in 2016 for the pre-launch validation of the satellite mission Aeolus. *Atmos. Meas. Tech.* **2018**, *11*, 3297–3322. [CrossRef]
11. Jung, T.; Gordon, N.D.; Bauer, P.; Bromwich, D.H.; Chevallier, M.; Day, J.J.; Dawson, J.; Doblas-Reyes, F.; Fairall, C.; Goessling, H.F.; et al. Advancing polar prediction capabilities on daily to seasonal time scales. *Bull. Am. Meteorol. Soc.* **2016**, *97*, 1631–1647. [CrossRef]
12. Shoupe, M.; de Boer, G.; Dethloff, K.; Hunke, E.; Maslowski, W.; McComiskey, A.; Perrson, O.; Randall, D.; Tjernstrom, M.; Turner, D.; et al. *The Multidisciplinary Drifting Observatory for the Study of Arctic Climate (MOSAIC) Atmosphere Science Plan*; DOE Office of Science Atmospheric Radiation Measurement (ARM) Program, Brookhaven National Laboratory: Upton, NY, USA, 2018.
13. Dörnbrack, A.; Weissmann, M.; Rahm, S.; Simmet, R.; Reitebuch, O.; Busen, R.; Olafsson, H. Wind Lidar Observations in the Lee of Greenland. In Proceedings of the 11th Conference on Mountain Meteorology, Bartlett, NH, USA, 20–25 June 2004.
14. Kavaya, M.J.; Beyon, J.Y.; Koch, G.J.; Petros, M.; Petzar, P.J.; Singh, U.N.; Trieu, B.C.; Yu, J. The Doppler Aerosol Wind Lidar (DAWN) airborne, wind-profiling, coherent-detection lidar system: Overview, flight results and plans. *J. Atmos. Ocean. Technol.* **2014**, *34*, 826. [CrossRef]
15. Black, P.; Harrison, L.; Beaubien, M.; Bluth, R.; Woods, R.; Penny, A.; Smith, R.W.; Doyle, J.D. High-definition sounding system (HDSS) for atmospheric profiling. *J. Atmos. Ocean. Technol.* **2017**, *34*, 777–796. [CrossRef]
16. Saha, S.; Moorthi, S.; Pan, H.L.; Wu, X.; Wang, J.; Nadiga, S.; Tripp, P.; Kistler, R.; Woollen, J.; Behringer, D.; et al. The NCEP climate forecast system reanalysis. *Bull. Am. Meteorol. Soc.* **2010**, *91*, 1015–1058. [CrossRef]
17. Hersbach, H.; De Rosnay, P.; Bell, B. *Operational Global Reanalysis: Progress, Future Directions and Synergies with NWP*; ERA Report Series 27; European Centre for Medium Range Weather Forecasts: Reading, UK, 2018; 65p.
18. Bromwich, D.H.; Wilson, A.B.; Bai, L.; Liu, Z.; Barlage, M.; Shih, C.F.; Maldonado, S.; Hines, K.M.; Wang, S.H.; Woollen, J.; et al. The Arctic system reanalysis, version 2. *Bull. Am. Meteorol. Soc.* **2018**, *99*, 805–828. [CrossRef]
19. Bromwich, D.H.; Wilson, A.B.; Bai, L.; Moore, G.W.K.; Bauer, P. A comparison of the regional Arctic System Reanalysis and the global ERA-Interim reanalysis for the Arctic. *Q. J. R. Meteorol. Soc.* **2016**, *142*, 644–658. [CrossRef]
20. Skamarock, W.C.; Klemp, J.B.; Dudhia, J.; Gill, D.O.; Barker, D.M.; Duda, M.G.; Huang, X.Y.; Wang, W.; Powers, J.G. A Description of the Advanced Research WRF Version 3, NCAR Technical Note. 2008. Available online: http://www.mmm.ucar.edu/wrf/users/docs/arw_v2Pdf (accessed on 25 May 2015).
21. Bromwich, D.H.; Hines, K.M.; Bai, L. Development and testing of Polar WRF: 2. Arctic Ocean. *J. Geophys. Res.* **2009**, *114*, D08122.
22. Hines, K.M.; Bromwich, D.H.; Bai, L.; Barlage, M.; Slater, A.G. Development and testing of Polar WRF. Part III. Arctic land. *J. Clim.* **2011**, *24*, 26–48. [CrossRef]
23. Powers, J.; Manning, K.W.; Bromwich, D.H.; Cassano, J.J.; Cayette, A.M. A decade of Antarctic science support through AMPS. *Bull. Am. Meteorol. Soc.* **2012**, *93*, 1699–1712. [CrossRef]
24. DuVivier, A.K.; Cassano, J.J.; Greco, S.; Emmitt, G.D. A case study of observed and modeled barrier flow in the Denmark Strait in May 2015. *Mon. Weather Rev.* **2017**, *145*, 2385–2404. [CrossRef]
25. Yu, J.; Trieu, B.C.; Modlin, E.A.; Singh, U.N.; Kavaya, M.J.; Chen, S.; Bai, Y.; Petzar, P.J.; Petros, M. 1 J/pulse Q-switched 2-micron solid-state laser. *Opt. Lett.* **2006**, *31*, 462. [CrossRef]
26. Singh, U.N.; Walsh, B.M.; Yu, J.; Petros, M.; Kavaya, M.J.; Refaat, T.F.; Barnes, N.P. 20 years of Tm, Ho: YLF and LuLF laser development for global winds measurements. *Opt. Mater. Express.* **2015**, *5*, 827. [CrossRef]
27. Koch, G.; Beyon, J.Y.; Cowen, L.J.; Kavaya, M.J.; Grant, M.S. Three-dimensional wind profiling of offshore wind energy areas with airborne Doppler lidar. *J. Appl. Remote Sens.* **2014**, *8*, 083662. [CrossRef]
28. Koch, G.; Beyon, J.Y.; Modlin, E.A.; Petzar, P.J.; Woll, S.; Petros, M.; Yu, J.; Kavaya, M.J. Side-scan Doppler lidar for offshore wind energy applications. *J. Appl. Remote Sens.* **2012**, *6*, 063562. [CrossRef]
29. Greco, S.; Emmitt, G.D.; Garstang, M.; Kavaya, M. Doppler Aerosol WiNd (DAWN) Lidar During CPEX 2017: Instrument performance and data utility. *Remote Sens.* **2020**, *12*, 2951. [CrossRef]
30. Liu, Z.; Kavaya, M.J.; Bedka, K.M. Coherent Doppler Wind Lidar data processing software and wind retrieval from the Aeolus Cal/Val field campaign. *AGUFM* **2019**, *2019*, A12A-07.

31. Doyle, J.D.; Moskaitis, J.R.; Feldmeier, J.W.; Ferek, R.J.; Beaubien, M.; Bell, M.M.; Cecil, D.L.; Creasey, R.L.; Duran, P.; Elsberry, R.L.; et al. A view of tropical cyclones from above: The tropical cyclone intensity experiment. *Bull. Am. Meteorol. Soc.* **2017**, *98*, 2113–2134. [CrossRef]
32. Creasey, R.L.; Elsberry, R.L. Tropical cyclone center positions from sequences of HDSS sondes deployed along high-altitude overpasses. *Weather Forecast.* **2017**, *32*, 317–325. [CrossRef]
33. Greco, S.; Emmitt, G.D.; Garstang, M.; Kavaya, M.; Pu, Z. Doppler Aerosol WiNd (DAWN) Lidar from CPEX 2017: Convective Process Studies and Comparisons with Other Wind Measurement Sensors and Numerical Models. In Proceedings of the 23rd Conference on Integrated Observing and Assimilation Systems for the Atmosphere, Oceans and Land Surface (IOAS-AOLS) Poster Session, Phoenix, AZ, USA, 8 January 2019.
34. Harden, B.E.; Renfrew, I.A.; Petersen, G.N. A climatology of wintertime barrier winds off southeast Greenland. *J. Clim.* **2011**, *24*, 4701–4717. [CrossRef]
35. Moore, G.W.K.; Renfrew, I.A. Tip jets and barrier winds: A QuikSCAT climatology of high wind speed events around Greenland. *J. Clim.* **2005**, *18*, 3713–3725. [CrossRef]
36. Moore, G.W. A new look at Greenland flow distortion and its impact on barrier flow, tip jets and coastal oceanography. *Geophys. Res. Lett.* **2012**, *39*, L22806. [CrossRef]
37. Moore, G.W.K.; Bromwich, D.H.; Wilson, A.B.; Renfrew, I.; Bai, L. Arctic system reanalysis improvements in topographically forced winds near Greenland. *Q. J. R. Meteorol. Soc.* **2016**, *142*, 2033–2045. [CrossRef]
38. Renfrew, I.A.; Outten, S.D.; Moore, G.W.K. An easterly tip jet off Cape Farewell, Greenland. I: Aircraft observations. *Q. J. R. Meteorol. Soc.* **2009**, *135*, 1919–1933. [CrossRef]
39. Doyle, J.D.; Shapiro, M.A. Flow response to large-scale topography: The Greenland tip jet. *Tellus* **1999**, *51A*, 728–748. [CrossRef]
40. Våge, K.; Spengler, T.; Davies, H.C.; Pickart, R.S. Multi-event analysis of the westerly Greenland tip jet based upon 45 winters in ERA-40. *Q. J. R. Meteorol. Soc.* **2009**, *135*, 1999–2011. [CrossRef]
41. Ohigashi, T.; Moore, K. Fine structure of a Greenland reverse tip jet: A numerical simulation. *Tellus A Dyn. Meteorol. Oceanogr.* **2008**, *61*, 512–526. [CrossRef]
42. Emmitt, G.D. Advanced processing of Airborne Doppler Wind Lidar wind measurements to resolve PBL circulations and near surface wind fields over the open ocean. In Proceedings of the AGU 100th Fall Meeting, A41L—Boundary Layer Clouds and Turbulence and Their Interaction with the Underlying Land or Ocean Surface Poster Session, San Francisco, CA, USA, 12 December 2019.